

# Salt Enrichment and Dynamics in the Interface of Supercooled Aqueous Droplets

Victor Kwan, Shoubhik R. Maiti, Ivan Saika-Voivod, and Styliani Consta\*



Cite This: *J. Am. Chem. Soc.* 2022, 144, 11148–11158



Read Online

ACCESS |



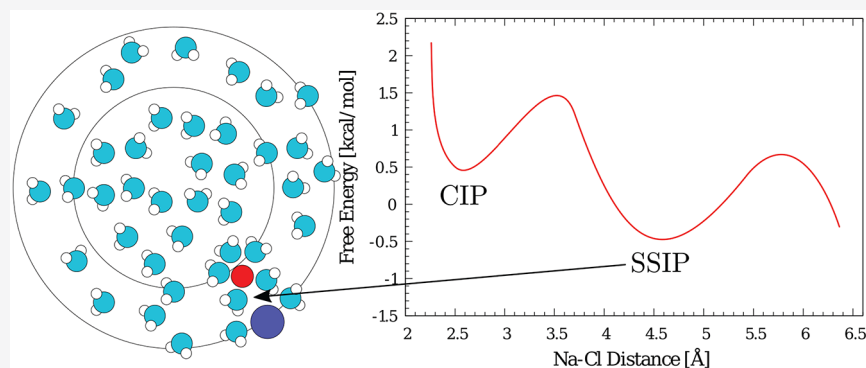
Metrics & More



Article Recommendations



Supporting Information



**ABSTRACT:** The interconversion reaction of NaCl between the contact-ion pair (CIP) and the solvent-separated ion pair (SSIP) as well as the free-ion state in cold droplets has not yet been investigated. We report direct computational evidence that the lower is the temperature, the closer to the surface the ion interconversion reaction takes place. In supercooled droplets the enrichment of the subsurface in salt becomes more evident. The stability of the SSIP relative to the CIP increases as the ion-pairing is transferred toward the droplet's outer layers. In the free-ion state, where the ions diffuse independently in the solution, the number density of  $\text{Cl}^-$  shows a broad maximum in the interior in addition to the well-known maximum in the surface. In the study of the reaction dynamics, we find a weak coupling between the interionic NaCl distance reaction coordinate and the solvent degrees of freedom, which contrasts with the diffusive crossing of the free energy barrier found in bulk solution modeling. The  $\text{H}_2\text{O}$  self-diffusion coefficient is found to be at least an order of magnitude larger than that in the bulk solution. We propose to exploit the enhanced surface ion concentration at low temperature to eliminate salts from droplets in native mass spectrometry ionization methods.

## INTRODUCTION

Cold droplets are characterized by distinct physical properties relative to their room temperature counterparts. A notable example is the preservation within nanodroplets of the supercooled liquid state, in contrast to the bulk, where practically unavoidable crystallization prevents the liquid from existing in the temperature range of  $T = 150$  to  $230$  K at  $P = 1$  atm of pressure.<sup>1–15</sup> In a broader context, the unique physical chemistry in small-volume cold systems has been demonstrated by the formation of new ice structures that cannot be seen in the bulk.<sup>1–12,16</sup>

Cold nano- and microdroplets have been studied through experiment and simulation in relation to crystallization and to their thermodynamic and structural properties.<sup>17–29,29,30</sup> These cold nanoscopic systems have a surprisingly complex internal structure that varies with temperature and size, as revealed by computer simulations of the TIP4P/2005 model of water,<sup>31–33</sup> which we now summarize in the context of the present study.

On cooling, and certainly by  $T = 220$  K, the outer water layers can become significantly denser compared to the interior of the droplet. The interior core density continues to follow

bulk values for the given  $T$  and interior  $P$ . For droplets with number of molecules  $N \geq 360$ , the droplet interior exhibits a temperature of maximum density below which the density decreases, creating a density contrast between the lower density core and higher density (sub)surface, a contrast that sharpens with decreasing  $T$ . For  $T \leq 200$ , the density differences between core and subsurface exceed 5%. The above scenario means that simulated supercooled droplets (for  $N \geq 200$ ) exhibit structural heterogeneity manifested by three radial regions: low-density interior, high-density subsurface (thickness  $\approx 0.7 - 0.8$  nm) and surface (thickness  $\approx 0.3$  nm). These regions are depicted in Figure 1. This structure provides an interesting chemical environment that contrasts with that of a

Received: January 29, 2022

Published: June 17, 2022



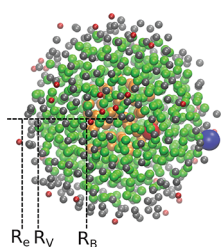


**Figure 1.** Typical snapshot of a supercooled droplet composed of  $N = 776$   $\text{H}_2\text{O}$  molecules and a sole  $\text{NaCl}$  ion pair. Only the O sites are depicted in the colored shells. The  $\text{Na}^+$  is depicted by the large red-colored sphere, and the  $\text{Cl}^-$  is depicted by the blue-colored sphere. The radii of the ions have been enlarged relative to the O sites for clarity. Three major regions are distinguished where the  $\text{H}_2\text{O}$  molecules are organized differently. Orange-colored interior: The water structure resembles the bulk. This region extends from the droplet center of mass (COM) to a distance  $r = R_B$  and is characterized by a lower density and a better formed tetrahedral network than the outer layers. Green-colored layer: This is the subsurface region where its distance  $r$  from the COM is in the range  $R_B < r < R_V$  and is characterized by a higher density and a lower degree of tetrahedrality than the interior. Gray-colored layer: This is the surface region in the range  $R_V < r < R_e$ , where  $R_e$  is the equimolar radius. The determination of  $R_B$  and  $R_V$  is presented in ref 33. A few  $\text{H}_2\text{O}$  molecules that their O sites are depicted by small red-colored spheres are found at  $r > R_e$ .

simpler nanodroplet at ambient conditions, where the density shows a decrease (mainly due to shape fluctuations) only at the liquid–vapor interface.

The exclusion of  $\text{NaCl}$  and other solutes by ice to its surface quasi-liquid layer (QLL) has been known for a long time.<sup>34–38</sup> This layer is the substrate for intense chemical reactivity. In analogy to that, the surface and subsurface of cold aerosols may host similar reactivity.<sup>35,39</sup> We present two examples that demonstrate the significance of the dynamics and thermodynamics of  $\text{NaCl}$  and other ions on the ice QLL. The first example is the effect of  $\text{NaCl}$  in the photolysis reactions of adsorbed polycyclic aromatic hydrocarbons.<sup>40,41</sup> The presence of  $\text{NaCl}$  in QLL has been found to affect the kinetics of the photolysis reactions, but the manner in which it intervenes is still unknown. The second example is the enhanced activity of hydronium ions on ice surfaces detected by thermal desorption mass spectrometry.<sup>42,43</sup> The experiments could not distinguish whether the activity was due to thermodynamic or kinetic factors,<sup>42,43</sup> which demonstrates the need to analyze both effects in order to understand the role of ions in reactivity. The interactions of salts and their dynamics in the outer layers of aerosols have not been explored yet at low temperature.

Here, we model the  $\text{NaCl}$  CIP  $\rightleftharpoons$  SSIP interconversion reaction, one of the fundamental reactions in chemistry, in mesoscopic clusters in the temperature range of 200–300 K. We also examine the number density of the free ions, which is the state where the ions are not engaged in the CIP and SSIP. The meaning of SSIP and CIP and free ions is the same as that traditionally defined in the literature.<sup>44–46</sup> The mesoscopic clusters are also called nanodroplets, and hereafter we will use the latter term.

Experiments and computations of  $\text{NaCl}$  ion-pairs in clusters have been mainly performed in systems composed of up to a few tens of  $\text{H}_2\text{O}$  molecules.<sup>47–57</sup> Fourier transform microwave spectroscopy<sup>51</sup> has shown that the distance between the ions in a  $\text{NaCl}$  pair increases by gradually adding up to 3  $\text{H}_2\text{O}$

molecules and reaches the value of 2.9 Å, which is the contact-ion pair (CIP) distance found in the bulk solution. Anion photoelectron spectroscopy<sup>52</sup> of clusters comprising  $\text{NaCl}$  and up to 12  $\text{H}_2\text{O}$  molecules found that at 9–12  $\text{H}_2\text{O}$  molecules, the CIP and SSIP (solvent-separated ion pair) formations are almost degenerate in energy. In larger clusters, characteristics different from those of minute or macroscopic sizes, such as the large shape fluctuations, prevail and may affect the reaction mechanisms. The experimental and computational studies of salt ion-pairing in larger clusters are more limited. Clusters of 150–400  $\text{H}_2\text{O}$  molecules containing  $\text{NaCl}$  have been studied by X-ray photoelectron spectroscopy.<sup>58,59</sup>

Nanodroplets are characterized by a large surface-to-volume ratio. Thus, when they are neutral and sufficiently large, they may have commonalities with the ion-pairing features in planar interfaces. The  $\text{NaCl}$  ion pairing in the planar water interface at room temperature has been extensively studied.<sup>40,46,53,60–80</sup> It has been found that the CIP and SSIP are stabilized differently in the interface from the bulk solution. There is a high degree of agreement that the ion dissociation is suppressed in the interface<sup>46,68,69</sup> relative to bulk solution.

The study of the ion pairing in cold systems is more challenging because of the slow dynamics.<sup>81,82</sup> The ion-pairing mechanism has been only recently explored in the premelting ice surface.<sup>83</sup> It has been found that the ice interface may play the dominant role in the reaction dynamics and that the dissociation dynamics of water molecules in the premelting layer differ significantly from those in bulk solution.

In this article we use the example of  $\text{NaCl}$  in an aqueous nanodroplet to examine via molecular modeling how the water structure and dynamics at cooling, and more evidently at supercooling, affect the ion-pairing. Different from the simulations of ion pairs in planar interfaces,<sup>46</sup> where the ions are restricted to remain in the interface, in the droplet simulations the ions are free to explore the entire volume. We hypothesize that the colder the droplet is the more likely it is for the CIP to SSIP interconversion reaction to occur in the droplet subsurface and surface. We also hypothesize that the location may affect the equilibrium constant. The dynamics in the droplets is characterized by the  $\text{H}_2\text{O}$  self-diffusion coefficient and the rate constant for the CIP to SSIP transition. As it will be discussed later, the salt enrichment of the interface at low temperature may be exploited to optimize the ionization conditions in mass spectrometry (MS).

## RESULTS AND DISCUSSION

**Equilibrium.** To examine how the particular structure of a cold droplet affects the ion-pairing, we mainly study systems comprising  $N = 776$   $\text{H}_2\text{O}$  molecules and a sole  $\text{NaCl}$  pair in the temperature range of 200–300 K. Droplets with  $N > 200$   $\text{H}_2\text{O}$  have sufficient number of  $\text{H}_2\text{O}$  molecules to form a surface, subsurface, and a bulk-like region allowing for the transferability of the results on ion solvation and ion-pairing to larger droplets. We model the systems with the TIP4P/2005 set of parameters and with the polarizable SWM4-NDP force field.<sup>84</sup> TIP4P/2005 allows one to model the systems at supercooling, but it lacks the electronic polarization. In previous research it has been found that the SWM4-NDP model yields nonphysical water density at low temperature,<sup>33,85,86</sup> and for this reason for this model, we can only study the trends in dynamic and equilibrium properties in the temperature range  $T = 260$ –300 K.

The TIP4P/2005 model shows that the number of transitions between CIP and SSIP as well as between SSIP and the free ions (Figure S1 in Supporting Information) is sufficient to provide good enough statistics to directly calculate free energy differences along the  $\text{Na}^+\text{--Cl}^-$  interionic distance. Indicatively, at  $T = 200$  K there are 7 transitions from CIP to SSIP within  $2.8 \mu\text{s}$ , and at  $T = 220$  K 10 transitions within  $0.8 \mu\text{s}$  (Figure S1 in Supporting Information). In Figure 2a (for the TIP4P/2005 model) the free energy along the  $\text{Na}^+\text{--Cl}^-$  interionic distance at  $T = 200$  and  $300$  K is shown. The CIP is defined within the basin where the  $\text{Na}^+\text{--Cl}^-$  interionic

distance is in the range of  $2.5\text{--}3.5 \text{ \AA}$ , the SSIP in  $3.5\text{--}5.7 \text{ \AA}$ , and the free ion state when the interionic distance is  $>5.7 \text{ \AA}$ . It is noted that the term “free ions” refers to the ions’ independent diffusive motion and not to lack of hydration. A SSIP may be easily formed (as is indicated by a very low free energy barrier along the interionic distance) by an encounter of the free ions in the course of their relative diffusive motion.<sup>44–46,87</sup> The equilibrium constant for  $\text{CIP} \rightleftharpoons \text{SSIP}$  and the free energy differences along the interionic distance are shown in Table 1. It is found that at  $T = 300$  K the CIP is stabilized more than at  $200$  K and that at  $200$  K, the free energy difference between CIP and SSIP is smaller than at  $300$  K.

Figure 2b and Figure 2c show the location at which the ion-pairing takes place at  $200$  and  $300$  K, respectively. The free-ion configurations account for  $\approx 70\%$  of the total number. In previous research<sup>33</sup> we have found that the supercooled droplets with  $N > 200$  exhibit heterogeneity that is manifested by three regions: a bulk-like interior, a subsurface, and a surface (Figure 1). In  $N = 776$  the distances from the droplet’s COM that delimit these regions are  $R_B = 7.4 \text{ \AA}$ ,  $R_V = 14.8 \text{ \AA}$ , and  $R_e = 17.7 \text{ \AA}$  (where  $R_e$  denotes the equimolar radius), respectively. At  $200$  K, the CIP and SSIP show a distinct propensity to be in the middle of the subsurface. In contrast, at  $300$  K, the probability of forming CIP and SSIP is significant throughout the volume of the droplet but still with a slightly higher probability in the subsurface. To quantify the orientation of the ion pairs, we consider the angle between the dipole moment of the CIP and SSIP (dipole moment is defined from the negative site to the positive site) and the vector defined from the droplet’s COM to the ion-pair COM. At  $T = 300$  K the orientation of the CIP spans all the angles, but at  $200$  K, the cosine of the angle peaks in the range  $0.0\text{--}0.2$ , which corresponds to an angle of  $90\text{--}78^\circ$  (Figure S2a in Supporting Information). The orientation of the NaCl is clearly more pronounced within the SWM4-NDP model (Figure S2b in Supporting Information). The CIP orientation indicates a slight preference of the  $\text{Cl}^-$  site toward the droplet’s surface. Even though Figure 2 only shows the  $\text{CIP} \rightleftharpoons \text{SSIP}$  equilibrium at two significantly different temperatures, the propensity of the ions to be in the subsurface increases gradually as the temperature decreases, as shown in Figure S3 and Figure S4 in Supporting Information. Specifically, we find that TIP4P/2005 at  $200$  K more strongly expels  $\text{Na}^+$  than  $\text{Cl}^-$  (Figure S4d in Supporting Information).

We think that the increased exclusion of the ions to the subsurface as temperature decreases is due to an improved H-bonded coordinated network in the droplet interior. The differences in the H-bonded network in the interior and subsurface in supercooled droplets have been presented in our previous research.<sup>33</sup> At supercooling, both the CIP and SSIP are mainly formed in the outer portion of the subsurface, where the dielectric constant is expected to be higher than that at  $300$  K. The higher dielectric constant at lower temperature may lead to a decrease in the free energy difference between the CIP and SSIP, which is consistent with the free energy profile at  $200$  K shown in Figure 2a.

Figure 3a shows the free energy of the interconversion between CIP and SSIP as a function of the NaCl interionic distance using the SWM4-NDP model. The  $K_{\text{eq}}$  values and the free energy differences are shown in Table 1. The striking feature is that the SSIP is formed with greater probability than the CIP. The free-ion configurations account for  $\approx 85\text{--}87\%$  of

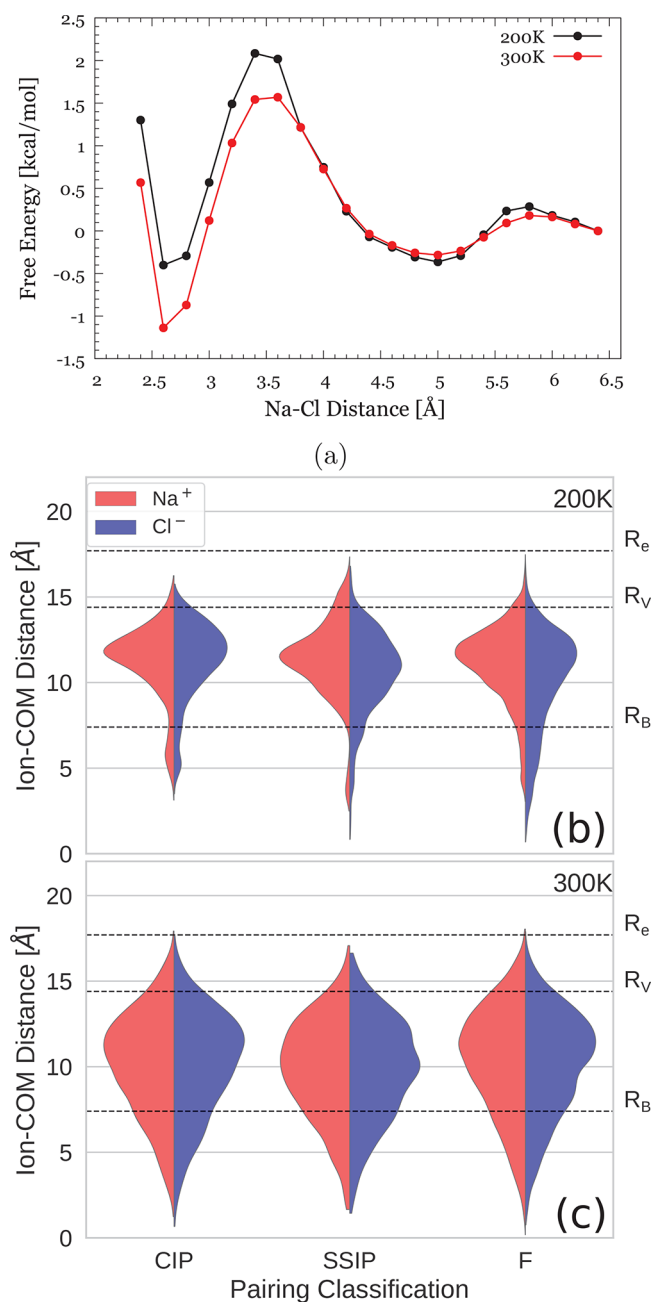


**Figure 2.** (a) Free energy for  $\text{CIP} \rightleftharpoons \text{SSIP}$  interconversion reaction at  $200$  and  $300$  K along the  $\text{Na}^+\text{--Cl}^-$  interionic distance. TIP4P/2005 model is used. (b) Probability distribution function for the distance between an ion and the droplet’s COM (y-axis) for  $\text{Na}^+$  (red) and  $\text{Cl}^-$  (blue) sites in the CIP, SSIP, and free ions (F) basins at  $200$  K. (c) Same as (b) but at  $300$  K.

**Table 1. Free Energy Differences ( $\Delta W_{1,2}$ ) between the Maximum and the Minima in the Free Energy Profiles Shown in Figure 2a and Figure 3a for TIP4P/2005 and SWM4-NDP Models, Respectively, at Various Temperatures<sup>a</sup>**

model	T [K]	$\Delta W_1$ [kcal/mol] ( $k_B T$ )		$\Delta W_2$ [kcal/mol] ( $k_B T$ )	$K_{eq}$
		CIP $\rightarrow$ BT		SSIP $\rightarrow$ BT	
TIP4P/2005	300	2.8 (4.7)		1.8 (3.0)	0.74
	260	2.6 (5.1)		2.1 (4.0)	1.09
	240	2.8 (5.8)		2.5 (5.2)	1.52
	210	2.3 (5.4)		2.1 (5.0)	1.92
	200	2.5 (6.3)		2.4 (6.0)	1.77
SWM4-NDP	300	1.4 (2.4)		2.2 (3.7)	10.2
	280	1.3 (2.3)		2.3 (4.1)	19.9
	260	1.3 (2.5)		2.3 (4.5)	22.5

<sup>a</sup>BT denotes the free energy barrier top along the interionic distance reaction coordinate. In the third and fourth columns, the number in parentheses is  $\Delta W_{1,2}$  in units of  $k_B T$ , where  $k_B$  is the Boltzmann constant. In the fifth column,  $K_{eq}$  is the equilibrium constant for CIP  $\rightleftharpoons$  SSIP. The statistical error in the free energy estimates is  $\pm 0.15$  kcal/mol.

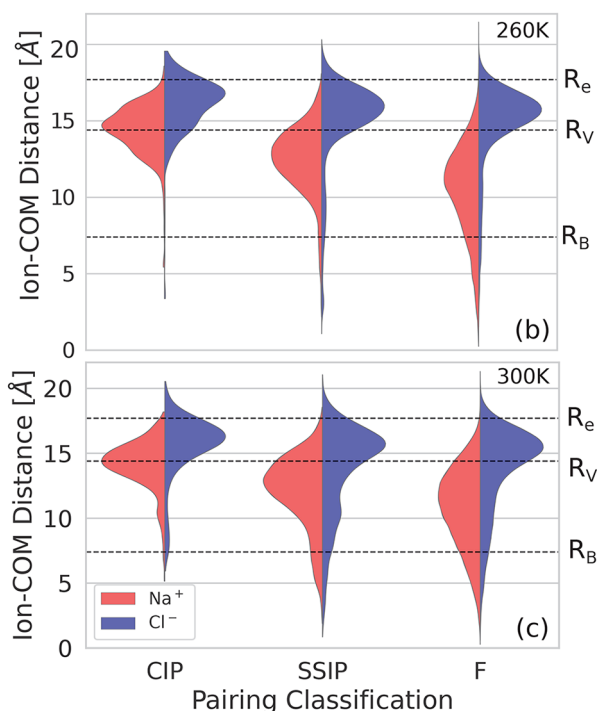
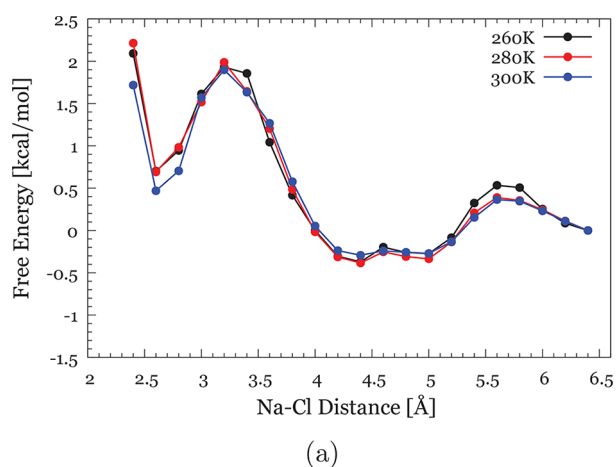


**Figure 3.** (a) Same as Figure 2a but for the SWM4-NDP polarizable model at various temperatures. (b) and (c) same as Figure 2b and Figure 2c, respectively, but for SWM4-NDP. Note that (b) is at 260 K, unlike in Figure 2b.

the total production run. Figure 3b and Figure 3c show that the CIP is formed near the surface at 300 and 260 K. The probability of encountering the ions in the interior and subsurface decreases considerably relative to the TIP4P/2005. The polarizable model finds the  $\text{Cl}^-$  to be nearer to the vapor–liquid interface than  $\text{Na}^+$ . The closer proximity of  $\text{Cl}^-$  to the surface is in agreement with previous studies<sup>49,53,88–90</sup> that have been performed at room temperature. The temperature effect, which has not been studied previously, shows that (a) the lower the temperature, the higher is the  $\text{Cl}^-$  number density in the surface (see also Figure S5 and Figure S6 in Supporting Information), (b) the free energy differences  $\Delta W_{1,2}(k_B T)$  (fourth column in Table 1) are not as sensitive to temperature as for TIP4P/2005. We attribute this reduced sensitivity to the fact that the polarizable model predicts the most probable location of the ions near the surface regardless of the temperature. We note that we have also performed simulations with different values of the Langevin damping (Figure S7 in Supporting Information), and all the free energy profiles are in agreement.

Here, we point out a significant difference in the relative stability of CIP and SSIP between the present study and that of Dang et al., who studied the ion-pairing in the liquid–vapor planar interface by using a polarizable model.<sup>46</sup> In the Dang et al. case, the ion pair was confined in the Gibbs dividing surface of the interface. It was found that the CIP is formed with a higher probability than the SSIP, whereas we find the opposite. We think that when the ion pair is confined in the Gibbs dividing surface, both  $\text{Na}^+$  and  $\text{Cl}^-$  are partially solvated, which promotes ion pairing due to the low dielectric constant environment. In our systems, the  $\text{Cl}^-$  lies on the surface, but the  $\text{Na}^+$  is well solvated at the borderline of the subsurface and surface or within the subsurface. The likelihood of the CIP formation relative to the SSIP may possibly decrease due to the particular requirements for the orientation of the  $\text{H}_2\text{O}$  molecules near the interface.

In summary, even though the polarizable and the non-polarizable force fields show different locations of the ion-pairing at room temperature, both models indicate that the lower the temperature is, the farther from the droplet's COM the ion pairing takes place. The models are also in agreement in that the stability of the SSIP relative to the CIP increases as the ion-pairing is transferred toward the droplet's outer layers and that when the CIP is formed, the  $\text{Cl}^-$  is found more in the exterior than when it is in the SSIP or free-ion form.

We would like now to discuss the consequences of the NaCl location for the reactivity of atmospheric aerosols. Donaldson et al. have detected<sup>41</sup> that brine exclusion to the surface quasi-liquid layer (QLL) of ice<sup>40,91</sup> affects the kinetics of photolysis reactions of adsorbed polycyclic aromatic hydrocarbons (e.g., anthracene, harmine). Similarly, it is expected that such organic molecules can also be adsorbed on aerosol surfaces. We suggest that the temperature-dependent spatial distribution of salts may be one of the factors that determine the photolysis kinetics in aerosols during different seasons or weather conditions. The precise mechanism in which the salts in the ice QLL affect the photolysis kinetics is still unknown.<sup>41</sup> One possible deduction from spectroscopic measurements by Donaldson et al. is that brine exclusion to the surface may form a similar environment to that of a concentrated aqueous bulk solution, making the photolysis reactions have the same kinetics as that in the bulk solution. The relation between the structure of a supersaturated bulk salt solution to that of the salt-containing QLL is still to be examined. We think that this similarity may not hold for fine and ultrafine cold atmospheric aerosols where the subsurface and surface (which can be considered the counterpart of QLL on ice) may have different thickness from that of bulk ice. The present study shows that more generally, in ultrafine aerosols, a low temperature where H<sub>2</sub>O is still liquid may affect to a different extent the brine concentration in the subsurface and the resulting ion-interconversion equilibrium constant and dynamics (described in the next section). Therefore, we expect that the kinetics of the photolysis reactions of organic compounds on fine and ultrafine atmospheric aerosols in the presence of salts may be determined by different factors from those on the ice surface.

**Solvation of CIP and SSIP.** Here we discuss the solvation of CIP and SSIP using the SWM4-NDP model. The distribution of the number of H<sub>2</sub>O molecules found in the closest hydration shell surrounding CIP and SSIP is shown in Figure S8 in Supporting Information, and the average values are presented in Table 2. In Table 2 the number of the oxygen

**Table 2. Average Number of Oxygen Sites in the First Hydration Shell Surrounding the Ion Pair<sup>a</sup>**

<i>T</i> [K]	CIP <sub>i</sub>	CIP <sub>s</sub>	SSIP <sub>i</sub>	SSIP <sub>s</sub>
300	8.06	6.80	10.44	9.26
280	7.75	6.56	10.18	9.30
260	7.50	6.89	9.98	9.28

<sup>a</sup>The averages correspond to the distributions shown in Figure S9. The subscripts *s* and *i* denote surface and interior, respectively.

sites were calculated within a distance of 3.9 Å from the Cl<sup>-</sup> ion or within 3.2 Å from the Na<sup>+</sup> ion. These distances are chosen to be the first minimum of the ion–oxygen radial distribution functions. We define the ion pair being on the surface (indicated by subscript *s* in CIP and SSIP in Table 2) if one or both ions are further than 17 Å from the droplet's COM (note: *R*<sub>0</sub> = 17.7 Å). We find that the ion pairs located on the surface are solvated by ≈1.2 fewer H<sub>2</sub>O molecules than in the interior in the range of 260–300 K. The number of H<sub>2</sub>O molecules in the nearest hydration shell decreases in the interior as the temperature decreases. We think that this decrease is due to the fact that the distance of 17 Å used to define the interior also includes the outer subsurface. At lower temperature, the ions have higher probability to be found in

the outer subsurface region where they may experience reduced solvation.

The SSIP basin (Figure 3a) is wide and shows a fine structure of two small local minima. This structure is consistent throughout the temperature range 260–300 K and agrees very well with the structure observed in the potential of mean force (PMF) reported by Dang et al. using a different polarizable model.<sup>46</sup> As we are going to see later, this structure is consistent even in the presence of four NaCl pairs. The fine SSIP structure is not seen by the nonpolarizable models, and even though it is present in the PMFs of Dang et al., they did not comment on it. The persistence of the fine structure indicates that it is a robust feature that we expect to be detected in spectroscopic signals. The hydration of the SSIP states corresponding to the small local minima is shown in Figure 4. We find that in the second local minimum the oxygen

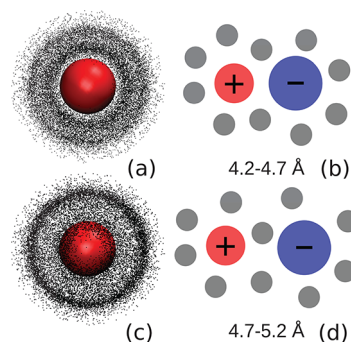


**Figure 4.** (a) Spatial distribution of oxygen sites (black dots) around the Na<sup>+</sup> ion (red sphere), viewed from the center of mass of the ion pair toward the Na<sup>+</sup> ion for interionic distance 4.2–4.7 Å projected on a 2D image. Only O sites within 3.2 Å from the Na<sup>+</sup> ion are included. It is noted that the Cl<sup>-</sup> ion is hidden behind the view point, and O sites behind the Na<sup>+</sup> are obscured by the Na<sup>+</sup> ion and are not shown. The O distribution is built from saved configurations of the MD trajectory. (b) Schematic representation of the O position at this interionic distance. (c) and (d) are the same as (a) and (b), respectively, but for interionic distance 4.7–5.2 Å. Distribution of H and O sites as shown in (a) and (c) are presented in Figure S9 in Supporting Information.

sites are nearer to the SSIP interionic distance (Figure 4d) than in the first minimum (Figure 4b); thus, they are the precursors of the dissociated free-ion state. The results show that the SSIP is not a single structure as it has often been assumed,<sup>62</sup> but it may be composed by a multitude of short-living structures that in a stepwise manner lead to the dissociated free-ion state. These intermediate states may be viewed as probes of the dynamics of H<sub>2</sub>O in different water models and in experiments.

**Free Ions.** In order to have a closer look at the free-ion state, we compare the Na<sup>+</sup> and Cl<sup>-</sup> number density with that of the sole ions using the SWM4-NDP model at 300 K as shown in Figure 5. The free-ion state is the most probable state of the ion pair (87% of the total number of configurations). We find that the Na<sup>+</sup> number density is higher in the interior, in agreement with previous research.<sup>33,92,93</sup> We computed the number density of Cl<sup>-</sup> at *T* = 300 K as a function of the distance from the droplet's COM. The number density shows two broad maxima. The basin of the one maximum near the surface extends from the subsurface to the surface region (1.2–1.9 Å) and corresponds to a free energy minimum of 1.7 *k*<sub>B</sub>*T* measured from the barrier top, which is located at 1.2 Å. This

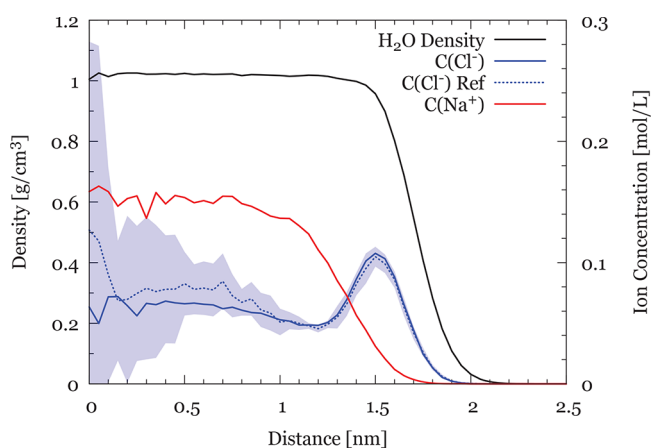


**Figure 5.** Number density profiles of  $\text{Na}^+$  and  $\text{Cl}^-$  sites (measured in units of concentration in the right  $y$ -axis) and  $\text{H}_2\text{O}$  density profiles (measured in units of  $\text{g}/\text{cm}^3$ ) in the left  $y$ -axis) at  $T = 300$  K in droplets comprising  $N = 776$   $\text{H}_2\text{O}$  molecules and a sole NaCl pair. For reference, the number density of a sole  $\text{Cl}^-$  in  $N = 776$  is included. The SWM4-NDP polarizable model is used.

free energy estimate is in good agreement with the value of  $\approx 1.0 k_B T$  reported by Caleman et al.<sup>92</sup> at  $T = 293.15$  K, using a version of the polarizable model near the one we employed here, in a cluster of radius equal to 1.1 nm, which corresponds to  $N \approx 190$   $\text{H}_2\text{O}$  molecules. The value of this free energy as a function of the distance from the droplet's COM is affected by shape fluctuations. The smaller the droplet, the larger is the effect. Our free energy estimate (as well as that of ref 92) includes the contribution from the purely entropic effect due to the spherical geometry. If the free energy due to the geometric effect is subtracted, then the effect due to the ion– $\text{H}_2\text{O}$  interactions equals  $0.90 k_B T$ . The  $N = 776$  droplet number density showed another broad maximum at  $0.7 \text{ \AA}$ . The basin that is associated with it is in the range of  $0.2\text{--}1.1 \text{ \AA}$ . It is likely that the basin extends up to the droplet's COM, but it is harder to distinguish that because of the larger statistical uncertainty near the center. To our knowledge the second maximum has not been previously discussed in the literature. The interior basin ( $0.2\text{--}1.2 \text{ \AA}$ ) corresponds to a free energy minimum that is more shallow than that on the surface, but it is wider, which indicates a substantial probability to encounter the  $\text{Cl}^-$  in the interior. The equilibrium constant estimated directly by the number of configurations in the exterior basin over the interior is 3.2; however, if we estimate the ratio of number densities in the two basins, then the value is 1.1. The presence of  $\text{Na}^+$  increases slightly the residence time of the  $\text{Cl}^-$  on the surface, which decreases the number density of the  $\text{Cl}^-$  in the interior.

**Multiple Ions.** To analyze the retention of salt in the interior of supercooled droplets, we also examined systems comprising 776  $\text{H}_2\text{O}$  molecules and four NaCl pairs, using the SWM4-NDP at 260 and 300 K and TIP4P/2005 at temperatures from 300 K down to 200 K. The probability density profiles (Figure S10 and Figure S11 in Supporting Information) and free energy profiles as a function of the interionic distance are shown in Figure S12 and Figure S13 in Supporting Information. The striking feature at lower temperature is the increased  $\text{Na}^+$  and  $\text{Cl}^-$  number density in the subsurface (distance from the COM  $>1.2$  nm) relative to that at 300 K. For SWM4-NDP the equilibrium constant as a ratio of configurations in the outer basin over the inner basin for  $\text{Cl}^-$

is 12.2 at 260 K versus 3.3 at 300 K. This ratio for  $\text{Na}^+$  is very similar at both temperatures and approximately equal to 0.84. The enrichment of the subsurface in ions at lower temperature is attributed to the exclusion of the ions from the bulk-like interior due to a better coordinated H-bonded network. The reduced shape fluctuations may contribute to this increase as well. We find here that the internal H-bonded network is maintained even at the higher concentration of NaCl. It is interesting to note that Figure S10 in Supporting Information may create the impression that at room temperature the ions are deeper in the interior measured from the surface than at lower temperature. The depth of the ions from the surface is the same at the various temperatures. The visual misconception arises from the fact that the distance from the COM order parameter masks the droplet's shape fluctuations. Comparison of the location of  $\text{Na}^+$  and  $\text{Cl}^-$  between the single pair in the droplet and the multiple pairs shows that in the higher NaCl concentration the ions have higher propensity toward the exterior. The free energy differences of CIP and SSIP (Figure S12 and Figure S13 in Supporting Information) are in excellent agreement with those for the single NaCl (Figure 3a and Table 1), which verifies the convergence of the runs.

It is interesting to note that for several ions in TIP4P/2005 we have consistently found that near  $R_B$  the probability density shows a minimum. This unfavorable region indicates the presence of an energetic barrier, arising from the different quality of the H-bonded network, in the crossing of the ion from the subsurface to the interior. We think that the presence of the ions can be used to probe the local environments at the water interface and interior and possibly to define the interface more precisely than any other order parameter.

Finally, we can examine the effect of the lower temperature on the location of the multiple ions in charged droplets, where ions of the same sign are in excess. We have studied droplets composed of 3000  $\text{H}_2\text{O}$  molecules and  $22\text{Na}^+ - 8\text{Cl}^-$  ions or  $22\text{Cl}^- - 8\text{Na}^+$  ions at  $T = 240$  and 300 K using TIP4P/2005. The data and analysis are presented in section S8 in Supporting Information. The key idea of the surface enrichment in salts also appears in the highly charged droplets. TIP4P/2005 shows the trend for the enrichment, and we expect that a polarizable model will show an even higher enhancement of the surface concentration. In native mass spectrometry (MS) droplets are heated up in order to quickly evaporate, but in this process ions may form undesirable adducts with the analytes. We propose that by initial cooling of a droplet instead of heating, or by introducing cycles of alternating heating and cooling during desolvation, the ions may accumulate near the surface. Cooling may also occur naturally via evaporation. Possibly, bombardment with other molecules may assist in the detachment of solvated ions or their salt complexes from the surface and reduce adduct formation at the latest stage of protein or other macromolecule desolvation.

**Dynamics.** The dynamics of the ion-pair interconversion reaction may be affected by the self-diffusion of the  $\text{H}_2\text{O}$  molecules. We compute the self-diffusion coefficient using the fluctuation–dissipation theorem where we combine a correlation function formalism with the macroscopic description of diffusion within a spherical cavity. The details of the method are described in the Experimental Section. The diffusion coefficient as a function of temperature is shown in Table 3 and Figure 6. An example of the decay of  $\langle \delta J_{k,l,m}^*(0) \delta J_{k,l,m}(t) \rangle$  is shown in Figure S15 in Supporting

**Table 3. Self-Diffusion Coefficient of H<sub>2</sub>O (Third Column) and Rate Coefficient ( $k_f$ ) of the Conversion of CIP to SSIP (Fourth Column) vs  $T$  for TIP4P/2005 and SWM4-NDP<sup>a</sup>**

model	$T$ [K]	$D$ [nm <sup>2</sup> /ns]	$k_f$ [1/ns]	$\tau$ [ns]	error in $\tau$
TIP4P/2005	300	53.1	7.04	0.142	0.007
	260	19.6	2.34	0.428	0.012
	220	6.01	0.19	5.360	0.112
SWM4-NDP	300	101.8	2.43	0.412	0.019
	280	47.0	0.64	1.561	0.048
	260	26.7	0.35	2.837	0.055

<sup>a</sup>Additional values of  $D$  at different  $T$  for TIP4P/2005 are shown in Table S4 in Supporting Information. As a reference, the experimental value of  $D$  for water is 2.30 nm<sup>2</sup>/ns at room temperature and SWM4-NDP has been parametrized to reproduce this value ( $2.33 \pm 0.02$  nm<sup>2</sup>/ns from ref 84).  $\tau$  is the dissociation lifetime ( $1/k_f$ ).

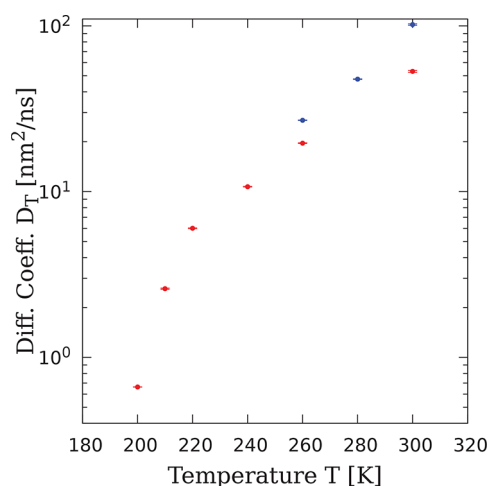


**Figure 6.** Diffusion coefficient of H<sub>2</sub>O as a function of temperature for  $N = 776$ . The red points are for TIP4P/2005 and the blue for SWM4-NDP.

**Information.** At  $T = 300$  K, both TIP4P/2005, which reproduces well the diffusion coefficient in bulk water for ambient and supercooled temperatures,<sup>94</sup> and SWM4-NDP predict a diffusion coefficient value approximately 23 and 44 times larger than that of the bulk at room temperature (exp  $D = 2.30$  nm<sup>2</sup>/ns), respectively. Near 200 K, the diffusion coefficient in the  $N = 776$  droplet approaches the experimental value of supercooled water<sup>95</sup> at 260.1 K.

We attribute these large  $D$  values relative to bulk water to the fact that in  $N = 776$  droplets, 93% of the molecules are found in the subsurface (411 H<sub>2</sub>O molecules out of 776) and surface (108 H<sub>2</sub>O molecules out of 776), where molecules often diffuse fast via a “jumping” mechanism,<sup>96,97</sup> which does not exist in bulk solution. The jumps occur within several picoseconds and they are facilitated by the shape fluctuations. The high value of diffusion coefficient is consistent with experimental suggestions that orders of magnitude reaction acceleration in microdroplets relative to the bulk solution may also indicate a significant increase in the value of the diffusion coefficient.<sup>98,99</sup> The diffusion coefficient is expected to be much higher in nanoscopic droplets because of the larger surface and shape fluctuations’ contributions.

We find the forward rate constant (CIP  $\rightarrow$  SSIP) by using the time evolution of the interionic distance of the MD trajectories. We compute the time-correlation function of a state variable  $n_{\text{CIP}}$  that has the value of 1 if the interionic

distance is less than 3.3 Å (for SWM4-NDP) and 0 if it is greater than this value. The correlation function is fitted to  $\phi(t) = p_{\text{CIP}} p_{\text{SSIP}} \exp(-k_f t) + p_{\text{CIP}} p_{\text{CIP}}$ , where  $p_{\text{CIP}}$  and  $p_{\text{SSIP}}$  denote probabilities of CIP and SSIP, respectively. An example of the decay of  $\langle n_{\text{CIP}}(t) n_{\text{CIP}}(0) \rangle$  is shown in Figure S16 in Supporting Information, and the values are presented in Table 3. The back rate constant (SSIP  $\rightarrow$  CIP) can be computed by  $k_b = k_f / K_{\text{eq}}$ , where  $K_{\text{eq}}$  is shown in Table 1. As expected, the reaction rate decreases with temperature for both models. Overall, the rate constant is higher in the TIP4P/2005 model than in SWM4-NDP. In SWM4-NDP, the transitions are very few but the lifetime of CIP is longer than in TIP4P/2005. The difference is attributed to the fact that in SWM4-NDP the CIP-SSIP transition occurs closer to the surface than in the TIP4P/2005. Near the surface it is expected for the CIP to live longer than in the TIP4P/2005 model because of the much lower dielectric constant in this location. The droplet electric field on the surface also may contribute in this stabilization because the ion pair is oriented with the negative site (Cl<sup>-</sup>) toward the hydrogen-site richer surface.

The dynamics of the interconversion reaction is affected by two factors that are not present in bulk solution. First, the Cl<sup>-</sup> is less solvated than the Na<sup>+</sup> ion since it is found almost at the surface; therefore, it is mainly the motions of the solvent molecules around Na<sup>+</sup> that determine the dynamics.<sup>49</sup> Second, diffusion of the solvent molecules is much faster in the droplet relative to the bulk, especially in the subsurface and surface. These factors may decrease the coupling of the interionic distance reaction coordinate with the solvent. As a result, no diffusive barrier crossing is found in the direct monitoring of the CIP-SSIP transitions. Figure S17 in Supporting Information shows representative trajectory segments with CIP-SSIP transitions from a trajectory at  $T = 260$  K using SWM4-NDP. Lack of diffusive motion at the barrier top is also found for TIP4P/2005, which shows that the weak coupling is extended in the entire subsurface. In contrast, in the bulk solution as it has been demonstrated by other authors<sup>44,46</sup> there is a strong coupling between the solvent and the interionic distance reaction coordinate, which leads to several recrossings at the barrier top of the free energy profile.

## CONCLUSION

The modeling of NaCl ion-pairing in aqueous nanodroplets shows that in colder droplets the pairing is more likely to take place near the surface. In this location the stability of the SSIP relative to the CIP increases. This is opposite the results of bulk solution simulations.<sup>46,68,69</sup> The polarizable model shows a substantial stabilization of the SSIP relative to CIP not only at low temperature but also at  $T = 300$  K. An important side-result of modeling via SWM4-NDP (polarizable model) is an interior broad maximum in the number density for the Cl<sup>-</sup> ion, when it is in the free ion form, in addition to the well-known maximum in the surface.<sup>92,93</sup> This result indicates that the nonpolarizable force fields overemphasize the interior local maximum.

In the study of the reaction dynamics, we found a weak coupling between the interionic NaCl distance reaction coordinate and the solvent degrees of freedom. The reduced coupling is mainly attributed to the presence of Cl<sup>-</sup> near the surface and to the fast diffusion of H<sub>2</sub>O molecules. In contrast to bulk solution where the crossing of the free energy barrier (along the interionic distance) is diffusive, there are no significant recrossings in droplets. We estimated the self-

diffusion of H<sub>2</sub>O by introducing a method that avoids the problems of employing mean-square displacement and the velocity autocorrelation function for computing the diffusion coefficient in spherical confined geometry. We found that the H<sub>2</sub>O self-diffusion coefficient at room temperature is at least an order of magnitude larger than that in bulk solution. The TIP4P/2005 model shows that it is at  $\approx 210$  K that the diffusion coefficient of H<sub>2</sub>O in the droplet equals the bulk value at room temperature.

In atmospheric chemistry, there are important but still unanswered questions about how the structure of the salt-containing quasi-liquid layer (QLL) on ice affects the kinetics of photolysis reactions of adsorbed polycyclic aromatic hydrocarbons.<sup>40,41</sup> Similar questions are expected about the role of NaCl in the photolysis reactions of adsorbed organic molecules on aerosols where their subsurface and surface can be considered the counterpart of QLL on ice. The present study provided thermodynamic and dynamic information to better understand the chemistry of salts in these outer layers.

We also envision application of this study in the field of mass spectrometry. Because of the shift in the location of ion distributions and ion-pairing with temperature, we propose to exploit a cycle of alternating low and high temperature as a way to control the adduct formation with macromolecules in droplet-based ionization methods used in mass spectrometry. Natural evaporative cooling may also contribute in the decrease of temperature in droplets. Bombardment of cold charged droplets with other molecules may be a possible way to remove Na<sup>+</sup> ions from the salt enriched interface. Enhanced salt release from droplets that carry the analytes may considerably extend the capability of native mass spectrometry analysis because it may allow for the salinity of the parent bulk solution of a biological sample to be closer to a physiological concentration of NaCl or KCl. Protons are another major ionic species in charged droplets. Experiments and computations have detected enhanced proton activity<sup>42,43</sup> on ice at 155 K. Molecular dynamics simulations predicted that the migration of surface-hydrated protons is  $\approx 2800$  slower than that of bulk protons at 190 K because they can be locally trapped by the undercoordinated water molecules.<sup>42,43</sup> Thus, it was deduced that the activity detected in experiments arises from the higher proton concentration.<sup>42,43</sup> It has also been found that protons are excluded from the ice bulk because of poor solubility in ice.<sup>100–102</sup> The present study and accumulated evidence from the literature on ice supports the hypothesis that protons in cold aqueous droplets will also be expelled to the surface and their migration may slow down due to local trapping. Therefore, the alternating cooling and heating of droplets may also provide a possible method of controlling the degree of protonation in proteins. We have shown that protonation and sodiation lead to different conformations of proteins,<sup>103</sup> and therefore the migration of ions and their nature may also affect the conformations. The dynamics of the various processes involved, such as proton transfer migration rates as a function of temperature and rate of conformational changes of proteins, have to be examined in order to be able to control the chemistry of the proteins within droplets.

## EXPERIMENTAL SECTION

Here we present the main points of the computational methods. A detailed account of the methodology is found in [section S1 of the Supporting Information](#). The systems that were simulated are shown in [Table S1 of the Supporting Information](#). We performed equilibrium

molecular dynamics (MD) simulations of aqueous nanodroplets (a) with a single NaCl pair, (b) with multiple NaCl pairs, and (c) charged with multiple Na<sup>+</sup> ions with a smaller number of Cl<sup>-</sup> counterions and vice versa.

The majority of the systems were composed of  $N = 776$  H<sub>2</sub>O molecules ( $R_c = 1.77$  nm) and a few with  $N = 3000$  H<sub>2</sub>O molecules ( $R_c = 2.78$  nm). We selected a droplet of  $N = 776$  H<sub>2</sub>O to do the majority of the computations because this size is large enough to clearly distinguish the bulk-like interior of a droplet from the subsurface and at the same time this size is computationally feasible to be studied at low temperature and with a polarizable model. The MD simulations were performed using the software NAMD v2.14,<sup>104</sup> and the trajectories were visualized using VMD 1.9.4a47.<sup>105</sup> The water molecules were modeled with the TIP4P/2005 (transferable intermolecular potential with four points) model<sup>106</sup> and the SWM4-NDP model.<sup>84</sup> The ion parameters are described in [section S1 of Supporting Information](#) and for the TIP4P/2005 are shown in [Table S2 of Supporting Information](#). The TIP4P/2005 simulations were performed in the temperature range 200–300 K and the SWM4-NDP simulations in 260–300 K.

**Computation of Diffusion Coefficient in Droplets.** Droplets present a confining environment that restricts the range of molecule movement. The use of common formulas that relate the diffusion coefficient to the integral of the velocity correlation function or, equivalently, to the mean-squared displacement poses certain difficulties. The problem has already been pointed out by Berne and co-workers<sup>107</sup> regarding the diffusion coefficient in finite-sized systems. Here we calculate the diffusion coefficient in a droplet using correlation function formalism and the macroscopic description of the diffusion in a spherical cavity.

The evolution of the molecule position is given by the Laplace equation with the Neumann boundary conditions

$$\frac{\partial P(\mathbf{r}, t)}{\partial t} = DV^2P(\mathbf{r}, t) \quad (1)$$

where  $P$  denotes probability density and  $D$  denotes the diffusion coefficient.

The general solution of the Laplace equation is

$$P(\mathbf{r}, t) = \sum_{\substack{k,l,m \\ |ml| \leq l}} B_{k,l,m} e^{-Dt/a_{k,l}^2} j_l(r/a_{k,l}) Y_{l,m}(\theta, \phi) \quad (2)$$

where  $B_{k,l,m}$  are the numerical coefficients determined by the initial conditions.  $r, \theta, \phi$  are the spherical polar coordinates corresponding to the molecule position  $\mathbf{r}$ .  $Y_{l,m}(\theta, \phi)$  is the spherical harmonics of order  $l$  and rank  $m$ .  $j_l$  is the spherical Bessel function of the first kind,  $a_{k,l}/R_0$  are the solutions of  $j_l'(x) = 0$  imposed by the Neumann boundary conditions, and  $R_0$  is the droplet's equimolar radius.

Using the orthonormality conditions for the spherical Bessel functions, we arrive at the identity

$$\begin{aligned} B_{k,l,m} e^{-Dt/a_{k,l}^2} &= \langle r^2 j_l(r/a_{k,l}) Y_{l,m}^*(\theta, \phi) \rangle \\ &= \int_{r \leq R_0} d^3\mathbf{r} r^2 j_l(r/a_{k,l}) Y_{l,m}^*(\theta, \phi) P(\mathbf{r}, t) \end{aligned} \quad (3)$$

We introduce a microscopic quantity  $\delta J_{k,l,m}$  corresponding to the decay of the probability density of the molecule location using the following identity

$$\delta J_{k,l,m}(t) = r^2 j_l(r_i(t)/a_{k,l}) Y_{l,m}(\theta_i(t), \phi_i(t)) \quad (4)$$

for a molecule  $i$ .

Using the linear response ansatz,<sup>108</sup> we equate the decay of the macroscopic expectation [3](#) to the single molecule autocorrelation function

$$\frac{a_{k,l}^2}{D} = \frac{1}{\langle \delta J_{k,l,m}^*(0) \delta J_{k,l,m}(0) \rangle} \times \int_0^\infty dt \langle \delta J_{k,l,m}^*(0) \delta J_{k,l,m}(t) \rangle \quad (5)$$

We use the spherical Bessel function of order  $l = 1$

$$j_1(x) = \frac{\sin x}{x} - \frac{\cos x}{x^2} \quad (6)$$

The first solution of the Neumann b.c. is  $a_{1,1} = 2.082R_0$ . From eq 5 we can find  $D$  by computing the time autocorrelation function (right-hand side of eq 5) from the MD trajectories and by using the value of  $a_{1,1}$ . The program for the computation of the diffusion coefficient has been prepared by SC.

## ASSOCIATED CONTENT

### Supporting Information

The Supporting Information is available free of charge at <https://pubs.acs.org/doi/10.1021/jacs.2c01159>.

(S1) Details of the models and simulation methods; (S2) time evolution of the  $\text{Na}^+$  and  $\text{Cl}^-$  distance from the droplet's COM and the interionic distance of a sole NaCl pair in a droplet of  $N = 776$   $\text{H}_2\text{O}$  molecules modeled with TIP4P/2005 at various temperatures; (S3) dipole moment orientation of NaCl; (S4)  $\text{Na}^+$  and  $\text{Cl}^-$  ion distribution profiles in the CIP, SSIP, and free ions formed in a droplet comprising 776 TIP4P/2005  $\text{H}_2\text{O}$  molecules–NaCl at various temperatures; (S5, S6) ion probability density profiles using SWM4-NDP; (S7) solvation of  $\text{Na}^+$  and  $\text{Cl}^-$  in a droplet of 776 SWM4-NDP  $\text{H}_2\text{O}$ –NaCl at 260 K, 280 K, 300 K; (S8) probability density profiles for droplets with 4 NaCl in a droplet of 776  $\text{H}_2\text{O}$  molecules modeled by SWM4-NDP; (S9) probability density profiles and discussion for highly charged cold droplets with counterions; (S10) dynamics showing diffusion coefficients and representative segments of trajectories (PDF)

## AUTHOR INFORMATION

### Corresponding Author

Styliani Consta – Department of Chemistry, The University of Western Ontario, London, Ontario N6A 5B7, Canada;  
orcid.org/0000-0001-8869-4155; Email: [sconstas@uwo.ca](mailto:sconstas@uwo.ca)

### Authors

Victor Kwan – Department of Chemistry, The University of Western Ontario, London, Ontario N6A 5B7, Canada  
Shoubhik R. Maiti – Department of Chemistry, The University of Western Ontario, London, Ontario N6A 5B7, Canada; Department of Chemistry, The University of Sheffield, Sheffield S3 7HF, United Kingdom  
Ivan Saika-Voivod – Department of Physics and Physical Oceanography, Memorial University of Newfoundland, St. John's A1B 3X7, Canada

Complete contact information is available at:  
<https://pubs.acs.org/10.1021/jacs.2c01159>

### Notes

The authors declare no competing financial interest.

## ACKNOWLEDGMENTS

S.C. thanks Dr. Anatoly Malevanets, The University of Western Ontario, for discussions on the stability of charged systems. V.K. acknowledges the province of Ontario and The University of Western Ontario for the Queen Elizabeth II Graduate Scholarship in Science and Technology. S.R.M. thanks a MITACS Globalink research internship scholarship held in the S.C. research lab. We acknowledge the financial

support from Natural Sciences and Engineering Research Council (Canada). Computational resources were provided by Compute Canada.

## REFERENCES

- (1) Bergman, R.; Swenson, J. Dynamics of supercooled water in confined geometry. *Nature* **2000**, *403*, 283–286.
- (2) Richert, R. Dynamics of nanoconfined supercooled liquids. *Annu. Rev. Phys. Chem.* **2011**, *62*, 65–84.
- (3) Christenson, H. K. Confinement effects on freezing and melting. *J. Phys.: Condens. Matter* **2001**, *13*, R95.
- (4) Alba-Simionesco, C.; Coasne, B.; Dosseh, G.; Dudziak, G.; Gubbins, K.; Radhakrishnan, R.; Sliwinski-Bartkowiak, M. Effects of confinement on freezing and melting. *J. Phys.: Condens. Matter* **2006**, *18*, R15.
- (5) Imrichová, K.; Veselý, L.; Gasser, T. M.; Loerting, T.; Neděla, V.; Heger, D. Vitrification and increase of basicity in between ice Ih crystals in rapidly frozen dilute NaCl aqueous solutions. *J. Chem. Phys.* **2019**, *151*, 014503.
- (6) Cervený, S.; Mallamace, F.; Swenson, J.; Vogel, M.; Xu, L. Confined water as model of supercooled water. *Chem. Rev.* **2016**, *116*, 7608–7625.
- (7) Kaneko, T.; Bai, J.; Akimoto, T.; Francisco, J. S.; Yasuoka, K.; Zeng, X. C. Phase behaviors of deeply supercooled bilayer water unseen in bulk water. *Proc. Natl. Acad. Sci. U.S.A.* **2018**, *115*, 4839–4844.
- (8) Jiang, J.; Gao, Y.; Zhu, W.; Liu, Y.; Zhu, C.; Francisco, J. S.; Zeng, X. C. First-principles molecular dynamics simulations of the spontaneous freezing transition of 2D water in a nanoslit. *J. Am. Chem. Soc.* **2021**, *143*, 8177–8183.
- (9) Kaneko, T.; Bai, J.; Yasuoka, K.; Mitsutake, A.; Zeng, X. C. New computational approach to determine liquid–solid phase equilibria of water confined to slit nanopores. *J. Chem. Theory Comput.* **2013**, *9*, 3299–3310.
- (10) Zhu, C.; Gao, Y.; Zhu, W.; Liu, Y.; Francisco, J. S.; Zeng, X. C. Computational prediction of novel ice phases: A perspective. *J. Phys. Chem. Lett.* **2020**, *11*, 7449–7461.
- (11) Koga, K.; Tanaka, H.; Zeng, X. First-order transition in confined water between high-density liquid and low-density amorphous phases. *Nature* **2000**, *408*, 564–567.
- (12) Fischer, J. K.; Sippel, P.; Denysenko, D.; Lunkenheimer, P.; Volkmer, D.; Loidl, A. Supercooled water confined in a metal-organic framework. *Commun. Phys.* **2020**, *3*, 95.
- (13) Gallo, P.; Bachler, J.; Bove, L. E.; Böhmer, R.; Camisasca, G.; Coronas, L. E.; Corti, H. R.; de Almeida Ribeiro, I.; de Koning, M.; Franzese, G.; et al. Advances in the study of supercooled water. *Eur. Phys. J. E* **2021**, *44*, 143.
- (14) Muralidharan, A.; Pratt, L.; Chaudhari, M.; Rempe, S. Quasi-chemical theory for anion hydration and specific ion effects:  $\text{Cl}^-$ (aq) vs.  $\text{F}^-$ (aq). *Chem. Phys. Lett.* **2019**, *737*, 100037.
- (15) Gallo, P.; Loerting, T.; Sciortino, F. Supercooled water: A polymorphic liquid with a cornucopia of behaviors. *J. Chem. Phys.* **2019**, *151*, 210401.
- (16) Zhong, J.; Kumar, M.; Anglada, J.; Martins-Costa, M.; Ruiz-Lopez, M.; Zeng, X. C.; Francisco, J. S. Atmospheric Spectroscopy and Photochemistry at Environmental Water Interfaces. *Annu. Rev. Physiol.* **2019**, *70*, 45–69.
- (17) Huang, J.; Bartell, L. S. Kinetics of homogeneous nucleation in the freezing of large water clusters. *J. Phys. Chem.* **1995**, *99*, 3924–3931.
- (18) Hock, C.; Schmidt, M.; Kuhnen, R.; Bartels, C.; Ma, L.; Haberland, H.; v.Issendorff, B. Calorimetric observation of the melting of free water nanoparticles at cryogenic temperatures. *Phys. Rev. Lett.* **2009**, *103*, 073401.
- (19) Pan, D.; Liu, L.-M.; Slater, B.; Michaelides, A.; Wang, E. Melting the ice: on the relation between melting temperature and size for nanoscale ice crystals. *ACS Nano* **2011**, *5*, 4562–4569.

- (20) Manka, A.; Pathak, H.; Tanimura, S.; Wölk, J.; Strey, R.; Wyslouzil, B. E. Freezing water in no-man's land. *Phys. Chem. Chem. Phys.* **2012**, *14*, 4505–4516.
- (21) Pradzynski, C. C.; Forck, R. M.; Zeuch, T.; Slavíček, P.; Buck, U. A fully size-resolved perspective on the crystallization of water clusters. *Science* **2012**, *337*, 1529–1532.
- (22) Johnston, J. C.; Molinero, V. Crystallization, melting, and structure of water nanoparticles at atmospherically relevant temperatures. *J. Am. Chem. Soc.* **2012**, *134*, 6650–6659.
- (23) Li, T.; Donadio, D.; Galli, G. Ice nucleation at the nanoscale probes no man's land of water. *Nat. Commun.* **2013**, *4*, 1887.
- (24) Bhabhe, A.; Pathak, H.; Wyslouzil, B. E. Freezing of heavy water (D<sub>2</sub>O) nanodroplets. *J. Phys. Chem. A* **2013**, *117*, 5472–5482.
- (25) Sellberg, J. A.; Huang, C.; McQueen, T. A.; Loh, N.; Laksmono, H.; Schlesinger, D.; Sierra, R.; Nordlund, D.; Hampton, C.; Starodub, D.; et al. Ultrafast X-ray probing of water structure below the homogeneous ice nucleation temperature. *Nature* **2014**, *510*, 381–384.
- (26) Factorovich, M. H.; Molinero, V.; Scherlis, D. A. Vapor pressure of water nanodroplets. *J. Am. Chem. Soc.* **2014**, *136*, 4508–4514.
- (27) Nandi, P. K.; Burnham, C. J.; Futera, Z.; English, N. J. Ice-amorphization of supercooled water nanodroplets in no man's land. *ACS Earth Space Chem.* **2017**, *1*, 187–196.
- (28) Amaya, A. J.; Wyslouzil, B. E. Ice nucleation rates near 225 K. *J. Chem. Phys.* **2018**, *148*, 084501.
- (29) Malek, S. M. A.; Poole, P. H.; Saika-Voivod, I. Surface tension of supercooled water nanodroplets from computer simulations. *J. Chem. Phys.* **2019**, *150*, 234507.
- (30) Esmaildoost, N.; Pathak, H.; Späh, A.; Lane, T. J.; Kim, K. H.; Yang, C.; Amann-Winkel, K.; Ladd-Parada, M.; Perakis, F.; Koliyadu, J.; et al. Anomalous temperature dependence of the experimental x-ray structure factor of supercooled water. *J. Chem. Phys.* **2021**, *155*, 214501.
- (31) Malek, S. M. A.; Poole, P. H.; Saika-Voivod, I. Thermodynamic and structural anomalies of water nanodroplets. *Nat. Commun.* **2018**, *9*, 2402.
- (32) Kwan, V.; Consta, S. Molecular Characterization of the Surface Excess Charge Layer in Droplets. *J. Am. Soc. Mass Spectrom.* **2021**, *32*, 33–45.
- (33) Malek, S. M. A.; Kwan, V.; Saika-Voivod, I.; Consta, S. Low density interior in supercooled aqueous nanodroplets expels ions to the subsurface. *J. Am. Chem. Soc.* **2021**, *143*, 13113–13123.
- (34) Hobbs, P. V. *Ice Physics*; Oxford Classic Texts in the Physical Sciences; Oxford University Press, 2010.
- (35) Makkonen, L. Salinity and growth rate of ice formed by sea spray. *Cold Regions Science and Technology* **1987**, *14*, 163–171.
- (36) Tsironi, I.; Schlesinger, D.; Späh, A.; Eriksson, L.; Segad, M.; Perakis, F. Brine rejection and hydrate formation upon freezing of NaCl aqueous solutions. *Phys. Chem. Chem. Phys.* **2020**, *22*, 7625–7632.
- (37) Vrbka, L.; Jungwirth, P. Brine rejection from freezing salt solutions: A molecular dynamics study. *Phys. Rev. Lett.* **2005**, *95*, 148501.
- (38) Conde, M.; Rovere, M.; Gallo, P. Spontaneous NaCl-doped ice at seawater conditions: Focus on the mechanisms of ion inclusion. *Phys. Chem. Chem. Phys.* **2017**, *19*, 9566–9574 (cited by 26).
- (39) Eun, H. J.; Ishiuchi, S.-i.; Baek, J. Y.; Lee, S.; Heo, J.; Fujii, M.; Kim, N. J. Cryogenic ion spectroscopy of adenine complexes containing alkali metal cations. *Phys. Chem. Chem. Phys.* **2021**, *23*, 6783–6790.
- (40) Bartels-Rausch, T.; Jacobi, H.-W.; Kahan, T. F.; Thomas, J. L.; Thomson, E. S.; Abbatt, J. P.; Ammann, M.; Blackford, J. R.; Bluhm, H.; Boxe, C.; et al. A review of air–ice chemical and physical interactions (AICI): liquids, quasi-liquids, and solids in snow. *Atmospheric Chem. Phys.* **2014**, *14*, 1587–1633.
- (41) Kahan, T.; Kwamena, N.-O.; Donaldson, D. Different photolysis kinetics at the surface of frozen freshwater vs. frozen salt solutions. *Atmospheric Chem. Phys.* **2010**, *10*, 10917–10922.
- (42) Kato, F.; Sugimoto, T.; Matsumoto, Y. Direct experimental evidence for markedly enhanced surface proton activity inherent to water ice. *J. Phys. Chem. Lett.* **2020**, *11*, 2524–2529.
- (43) Park, K.; Lin, W.; Paesani, F. Fast and slow proton transfer in ice: The role of the quasi-liquid layer and hydrogen-bond network. *J. Phys. Chem. B* **2014**, *118*, 8081–8089.
- (44) Ciccotti, G.; Ferrario, M.; Hynes, J. T.; Kapral, R. Dynamics of ion pair interconversion in a polar solvent. *J. Chem. Phys.* **1990**, *93*, 7137–7147.
- (45) Guardia, E.; Rey, R.; Padró, J. Potential of mean force by constrained molecular dynamics: a sodium chloride ion-pair in water. *Chem. Phys.* **1991**, *155*, 187–195.
- (46) Dang, L. X.; Schenter, G. K.; Wick, C. D. Rate theory of ion pairing at the water liquid–vapor interface. *J. Phys. Chem. C* **2017**, *121*, 10018–10026.
- (47) Laria, D.; Fernández-Prini, R. Molecular dynamics study of water clusters containing ion pairs: From contact to dissociation. *J. Chem. Phys.* **1995**, *102*, 7664–7673.
- (48) Laria, D.; Fernández-Prini, R. Ion-pair solvation in aqueous clusters. *Chem. Phys. Lett.* **1993**, *205*, 260–266.
- (49) Consta, S.; Kapral, R. Ionization reactions of ion complexes in mesoscopic water clusters. *J. Chem. Phys.* **1999**, *111*, 10183–10191.
- (50) Zidi, Z. Solvation of sodium-chloride ion pair in water cluster at atmospheric conditions: Grand canonical ensemble Monte Carlo simulation. *J. Chem. Phys.* **2005**, *123*, 064309.
- (51) Mizoguchi, A.; Ohshima, Y.; Endo, Y. Microscopic hydration of the sodium chloride ion pair. *J. Am. Chem. Soc.* **2003**, *125*, 1716–1717.
- (52) Hou, G.-L.; Liu, C.-W.; Li, R.-Z.; Xu, H.-G.; Gao, Y. Q.; Zheng, W.-J. Emergence of solvent-separated Na<sup>+</sup>–Cl<sup>–</sup> ion pair in salt water: Photoelectron spectroscopy and theoretical calculations. *J. Phys. Chem. Lett.* **2017**, *8*, 13–20.
- (53) Knipping, E.; Lakin, M.; Foster, K.; Jungwirth, P.; Tobias, D.; Gerber, R.; Dabdub, D.; Finlayson-Pitts, B. Experiments and simulations of ion-enhanced interfacial chemistry on aqueous NaCl aerosols. *Science* **2000**, *288*, 301–306.
- (54) Perera, L.; Berkowitz, M. L. Many-body effects in molecular dynamics simulations of Na<sup>+</sup> (H<sub>2</sub>O)<sub>n</sub> and Cl<sup>–</sup>(H<sub>2</sub>O)<sub>n</sub> clusters. *J. Chem. Phys.* **1991**, *95*, 1954–1963.
- (55) Tandy, J.; Feng, C.; Boatwright, A.; Sarma, G.; Sadoon, A. M.; Shirley, A.; Das Neves Rodrigues, N.; Cunningham, E. M.; Yang, S.; Ellis, A. M. Communication: Infrared spectroscopy of salt-water complexes. *J. Chem. Phys.* **2016**, *144*, 121103.
- (56) Heindel, J. P.; Xantheas, S. S. The many-body expansion for aqueous systems revisited: II. Alkali metal and halide ion–water interactions. *J. Chem. Theory Comput.* **2021**, *17*, 2200–2216.
- (57) Herman, K. M.; Heindel, J. P.; Xantheas, S. S. The many-body expansion for aqueous systems revisited: III. Hofmeister ion–water interactions. *Phys. Chem. Chem. Phys.* **2021**, *23*, 11196–11210.
- (58) Partanen, L.; Mikkilä, M.-H.; Huttula, M.; Tchapyguine, M.; Zhang, C.; Andersson, T.; Björneholm, O. Solvation at nanoscale: Alkali-halides in water clusters. *J. Chem. Phys.* **2013**, *138*, 044301.
- (59) Smith, J. W.; Saykally, R. J. Soft x-ray absorption spectroscopy of liquids and solutions. *Chem. Rev.* **2017**, *117*, 13909–13934.
- (60) Ruiz-Lopez, M. F.; Francisco, J. S.; Martins-Costa, M. T.; Anglada, J. M. Molecular reactions at aqueous interfaces. *Nat. Rev. Chem.* **2020**, *4*, 459–475.
- (61) Jungwirth, P.; Finlayson-Pitts, B. J.; Tobias, D. J. Introduction: Structure and chemistry at aqueous interfaces. *Chem. Rev.* **2006**, *106*, 1137–1139.
- (62) Brini, E.; Fennell, C. J.; Fernandez-Serra, M.; Hribar-Lee, B.; Luksic, M.; Dill, K. A. How water's properties are encoded in its molecular structure and energies. *Chem. Rev.* **2017**, *117*, 12385–12414.
- (63) Björneholm, O.; Hansen, M. H.; Hodgson, A.; Liu, L.-M.; Limmer, D. T.; Michaelides, A.; Pedevilla, P.; Rossmeisl, J.; Shen, H.; Tocci, G.; et al. Water at interfaces. *Chem. Rev.* **2016**, *116*, 7698–7726.

- (64) Vaida, V. Perspective: Water cluster mediated atmospheric chemistry. *J. Chem. Phys.* **2011**, *135*, 020901.
- (65) Saykally, R. J. Two sides of the acid–base story. *Nat. Chem.* **2013**, *5*, 82–84.
- (66) Agmon, N.; Bakker, H. J.; Campen, R. K.; Henchman, R. H.; Pohl, P.; Roke, S.; Thämer, M.; Hassanal, A. Protons and hydroxide ions in aqueous systems. *Chem. Rev.* **2016**, *116*, 7642–7672.
- (67) Enami, S.; Colussi, A. J. Ion-Specific Long-Range Correlations on Interfacial Water Driven by Hydrogen Bond Fluctuations. *J. Phys. Chem. B* **2014**, *118*, 1861–1866.
- (68) Venkateshwaran, V.; Vembanur, S.; Garde, S. Water-mediated ion–ion interactions are enhanced at the water vapor–liquid interface. *Proc. Natl. Acad. Sci. U.S.A.* **2014**, *111*, 8729–8734.
- (69) Wick, C. D. NaCl dissociation dynamics at the air–water interface. *J. Phys. Chem. C* **2009**, *113*, 2497–2502.
- (70) Otten, D.; Onorato, R.; Michaels, R.; Goodknight, J.; Saykally, R. Strong surface adsorption of aqueous sodium nitrite as an ion pair. *Chem. Phys. Lett.* **2012**, *519*, 45–48.
- (71) Hua, W.; Verreault, D.; Huang, Z.; Adams, E. M.; Allen, H. C. Cation effects on interfacial water organization of aqueous chloride solutions. I. Monovalent cations: Li<sup>+</sup>, Na<sup>+</sup>, K<sup>+</sup>, and NH<sub>4</sub><sup>+</sup>. *J. Phys. Chem. B* **2014**, *118*, 8433–8440.
- (72) Schweighofer, K.; Benjamin, I. Ion pairing and dissociation at liquid/liquid interfaces: Molecular dynamics and continuum models. *J. Chem. Phys.* **2000**, *112*, 1474–1482.
- (73) Wick, C. D.; Kuo, I.-F. W.; Mundy, C. J.; Dang, L. X. The effect of polarizability for understanding the molecular structure of aqueous interfaces. *J. Chem. Theory Comput.* **2007**, *3*, 2002–2010.
- (74) Luo, G.; Bu, W.; Mihaylov, M.; Kuzmenko, I.; Schlossman, M. L.; Soderholm, L. X-ray reflectivity reveals a nonmonotonic ion-density profile perpendicular to the surface of ercl3 aqueous solutions. *J. Phys. Chem. C* **2013**, *117*, 19082–19090.
- (75) Chakraborty, D.; Patey, G. How crystals nucleate and grow in aqueous NaCl solution. *J. Phys. Chem. Lett.* **2013**, *4*, 573–578.
- (76) Als-Nielsen, J.; Jacquemain, D.; Kjaer, K.; Leveiller, F.; Lahav, M.; Leiserowitz, L. Principles and applications of grazing incidence x-ray and neutron scattering from ordered molecular monolayers at the air-water interface. *Phys. Rep.* **1994**, *246*, 251–313.
- (77) Winter, B. Liquid microjet for photoelectron spectroscopy. *Nucl. Instrum. Methods Phys. Res., Sect. A* **2009**, *601*, 139–150.
- (78) Stefaniu, C.; Brezesinski, G. X-ray investigation of monolayers formed at the soft air/water interface. *Curr. Opin. Colloid Interface Sci.* **2014**, *19*, 216–227.
- (79) Johnson, C. M.; Baldelli, S. Vibrational sum frequency spectroscopy studies of the influence of solutes and phospholipids at vapor/water interfaces relevant to biological and environmental systems. *Chem. Rev.* **2014**, *114*, 8416–8446.
- (80) Olivieri, G.; Parry, K. M.; D'Auria, R.; Tobias, D. J.; Brown, M. A. Specific anion effects on Na<sup>+</sup> adsorption at the aqueous solution–air interface: MD simulations, SESSA calculations, and photoelectron spectroscopy experiments. *J. Phys. Chem. B* **2018**, *122*, 910–918.
- (81) Misbah, C.; Müller-Krumbhaar, H.; Temkin, D. Interface structure at large supercooling. *J. Phys. I* **1991**, *1*, 585–601.
- (82) Singh, R. S.; Palmer, J. C.; Panagiotopoulos, A. Z.; Debenedetti, P. G. Thermodynamic analysis of the stability of planar interfaces between coexisting phases and its application to supercooled water. *J. Chem. Phys.* **2019**, *150*, 224503.
- (83) Niblett, S. P.; Limmer, D. T. Ion dissociation dynamics in an aqueous premelting layer. *J. Phys. Chem. B* **2021**, *125*, 2174–2181.
- (84) Lamoureux, G.; Harder, E.; Vorobyov, I. V.; Roux, B.; MacKerell, A. D. A polarizable model of water for molecular dynamics simulations of biomolecules. *Chem. Phys. Lett.* **2006**, *418*, 245–249.
- (85) Gladich, I.; Roeselová, M. Comparison of selected polarizable and nonpolarizable water models in molecular dynamics simulations of ice Ih. *Phys. Chem. Chem. Phys.* **2012**, *14*, 11371–11385.
- (86) Muchova, E.; Gladich, I.; Picaud, S.; Hoang, P. N.; Roeselová, M. The Ice-Vapor Interface and the Melting Point of Ice Ih for the Polarizable POL3 Water Model. *J. Phys. Chem. A* **2011**, *115*, 5973–5982.
- (87) Ciccotti, G.; Ferrario, M.; Hynes, J. T.; Kapral, R. Constrained molecular dynamics and the mean potential for an ion pair in a polar solvent. *Chem. Phys.* **1989**, *129*, 241–251.
- (88) Wilson, M. A.; Pohorille, A. Interaction of monovalent ions with the water liquid–vapor interface: A molecular dynamics study. *J. Chem. Phys.* **1991**, *95*, 6005–6013.
- (89) Perera, L.; Berkowitz, M. L. Structure and dynamics of Cl–(H<sub>2</sub>O) 20 clusters: The effect of the polarizability and the charge of the ion. *J. Chem. Phys.* **1992**, *96*, 8288–8294.
- (90) Werhahn, J. C.; Akase, D.; Xantheas, S. S. Universal scaling of potential energy functions describing intermolecular interactions. II. The halide-water and alkali metal-water interactions. *J. Chem. Phys.* **2014**, *141*, 064118.
- (91) Bartels-Rausch, T.; Kong, X.; Orlando, F.; Artiglia, L.; Waldner, A.; Huthwelker, T.; Ammann, M. Interfacial supercooling and the precipitation of hydrohalite in frozen NaCl solutions as seen by X-ray absorption spectroscopy. *Cryosphere* **2021**, *15*, 2001–2020.
- (92) Coleman, C.; Hub, J. S.; van Maaren, P. J.; van der Spoel, D. Atomistic simulation of ion solvation in water explains surface preference of halides. *Proc. Natl. Acad. Sci. U.S.A.* **2011**, *108*, 6838–6842.
- (93) Burnham, C. J.; Petersen, M. K.; Day, T. J.; Iyengar, S. S.; Voth, G. A. The properties of ion-water clusters. II. Solvation structures of Na<sup>+</sup>, Cl<sup>–</sup>, and H<sup>+</sup> clusters as a function of temperature. *J. Chem. Phys.* **2006**, *124*, 024327.
- (94) Rozmanov, D.; Kusalik, P. G. Transport coefficients of the TIP4P-2005 water model. *J. Chem. Phys.* **2012**, *136*, 044507.
- (95) Price, W. S.; Ide, H.; Arata, Y. Self-diffusion of supercooled water to 238 K using PGSE NMR diffusion measurements. *J. Phys. Chem. A* **1999**, *103*, 448–450.
- (96) Beck, T. L.; Berry, R. S. The interplay of structure and dynamics in the melting of small clusters. *J. Chem. Phys.* **1988**, *88*, 3910–3922.
- (97) Braun, O.; Ferrando, R. Role of long jumps in surface diffusion. *Phys. Rev. E* **2002**, *65*, 061107.
- (98) Lhee, S.; Lee, J. K.; Kang, J.; Kato, S.; Kim, S.; Zare, R. N.; Nam, H. G. Spatial localization of charged molecules by salt ions in oil-confined water microdroplets. *Sci. Adv.* **2020**, *6*, No. eaba0181.
- (99) Wei, Z.; Li, Y.; Cooks, R. G.; Yan, X. Accelerated reaction kinetics in microdroplets: Overview and recent developments. *Annu. Rev. Phys. Chem.* **2020**, *71*, 31–51.
- (100) Lee, D. H.; Kang, H. Proton transport and related chemical processes of ice. *J. Phys. Chem. B* **2021**, *125*, 8270–8281.
- (101) Schwartz, A. J.; Pollack, G. H. Ice-melting dynamics: The role of protons and interfacial geometry. *Langmuir* **2017**, *33*, 5585–5591.
- (102) Cowin, J.; Tsekouras, A.; Iedema, M.; Wu, K.; Ellison, G. Immobility of protons in ice from 30 to 190 K. *Nature* **1999**, *398*, 405–407.
- (103) Consta, S.; In Oh, M.; Kwan, V.; Malevanets, A. Strengths and weaknesses of molecular simulations of electrosprayed droplets. *J. Am. Soc. Mass Spectrom.* **2018**, *29*, 2287–2296.
- (104) Phillips, J. C.; Braun, R.; Wang, W.; Gumbart, J.; Tajkhorshid, E.; Villa, E.; Chipot, C.; Skeel, R. D.; Kalé, L.; Schulten, K. Scalable molecular dynamics with NAMD. *J. Comput. Chem.* **2005**, *26*, 1781–1802.
- (105) Humphrey, W.; Dalke, A.; Schulten, K. VMD: Visual Molecular Dynamics. *J. Mol. Graphics* **1996**, *14*, 33–38.
- (106) Abascal, J. L. F.; Vega, C. A general purpose model for the condensed phases of water: TIP4P/2005. *J. Chem. Phys.* **2005**, *123*, 234505.
- (107) Liu, P.; Harder, E.; Berne, B. On the calculation of diffusion coefficients in confined fluids and interfaces with an application to the liquid–vapor interface of water. *J. Phys. Chem. B* **2004**, *108*, 6595–6602.
- (108) Chandler, D. *Introduction to Modern Statistical Mechanics*; Oxford University Press, New York, 1987.

**Supporting Information:**

**Salt Enrichment and Dynamics in the Interface  
of Supercooled Aqueous Droplets**

Victor Kwan,<sup>†</sup> Shoubhik R Maiti,<sup>†,‡</sup> Ivan Saika-Voivod,<sup>¶</sup> and Styliani Consta<sup>\*,†</sup>

<sup>†</sup> *Department of Chemistry, The University of Western Ontario, London, Ontario, Canada  
N6A 5B7*

<sup>‡</sup> *Department of Chemistry, The University of Sheffield, Sheffield S3 7HF, United Kingdom*

<sup>¶</sup> *Department of Physics and Physical Oceanography, Memorial University of  
Newfoundland, Canada, A1B 3X7*

E-mail: [sconstas@uwo.ca](mailto:sconstas@uwo.ca)

# S1. Models and simulation methods

The MD simulations were performed using the software NAMD v2.14.<sup>S1</sup> The composition of the systems that were simulated, their dimension and length of simulation time are presented in Table S1. The simulation protocol is similar to that presented in Ref.<sup>S2</sup> but with a few differences. One difference is that droplets at  $T < 240$  K were simulated in vacuo (without a spherical boundary condition that we usually use<sup>S2</sup>) because they do not evaporate within the simulation time. Nanodroplets at  $T > 240$  K were placed in a spherical cavity of radius 20.0 nm by using a spherical boundary condition.<sup>S2</sup> The simulations were carried out in the canonical ensemble – constant number of molecules ( $N$ ), volume, and  $T$ . The systems were thermalized with the Langevin thermostat with the damping coefficient set to 1/ps, 0.1/ps and 0.01/ps. The equilibrium properties were computed with damping coefficient 1/ps, and we tested that they are independent of the value of the Langevin damping in the range of 1/ps-0.01/ps. The dynamics is performed with values of the damping coefficient in the range of 0.1/ps - 0.01/ps or without the coupling with a thermostat. All the simulation included a 0.2  $\mu$ s equilibration period followed by a 1.0  $\mu$ s - 3.0  $\mu$ s production run, with configurations sampled every 0.1 ns.

The systems were modeled with the TIP4P/2005 H<sub>2</sub>O model and with a Drude oscillator-based polarizable model. In the polarizable model the H<sub>2</sub>O molecules were represented with the SWM4-NDP model<sup>S3</sup> and the ions, Na<sup>+</sup> and Cl<sup>-</sup> with the CHARMM Drude force field.<sup>S4,S5</sup> The equations of motion for the TIP4P/2005 set of simulations were integrated with a time step of 2.0 fs and for the SWM4-NDP model with 1.0 fs.

**Annealing** To confirm the equilibration of the droplet simulated annealing was done on a pure water nanodroplet containing  $N = 777$  H<sub>2</sub>O molecules. The simulation was started at 320 K and the temperature was reduced in steps of  $-5$  K, with 2 ns equilibration time in each step. After the temperature went below 230 K, 8 ns equilibration time was allowed for each step. After the simulation reached 200 K, it was run at constant  $T$  for 15 ns. The

**Table S1: Description of systems studied.**  $N$  denotes the total number of water molecules in the system, the asterisk in the number of  $\text{H}_2\text{O}$  molecules denotes the runs with the SWM4-NDP polarizable model, “Ions” is the number and type of ions in the droplet,  $T$  [K] denotes the temperature of the system,  $N_d$  denotes the average number of water molecules that form the connected droplet,  $R_e$  denotes the equimolar radius of the droplet assuming  $1 \text{ g/cm}^3$  density,  $t_{run}$  is the production time for the system. For each system multiple runs have been performed with different values of the Langevin coupling.

$N$ ( $\text{H}_2\text{O}$ )	Ions	$T$ [K]	$N_d$	$R_e$ [nm]	$t_{run}$ [ $\mu\text{s}$ ]
776*	$1\text{Cl}^-$	240	770	1.77	0.8
		300	766	1.77	0.8
776	$1\text{Cl}^-$	200	776	1.77	3.8
776	$1\text{Na}^+, 1\text{Cl}^-$	200	776	1.77	2.8
		300	766.5	1.77	1
776*	$1\text{Na}^+, 1\text{Cl}^-$	260	770	1.77	0.1
		280	766	1.77	0.1
		300	766	1.77	0.5
776	$4\text{Na}^+, 4\text{Cl}^-$	200	776	1.77	1.8
		300	767.7	1.76	1
776*	$4\text{Na}^+, 4\text{Cl}^-$	260	776	1.77	0.8
		300	767.7	1.76	0.8
3000	$24\text{Na}^+, 8\text{Cl}^-$	240	3000	2.78	0.8
		300	3000	2.78	0.2
3000	$8\text{Na}^+, 24\text{Cl}^-$	240	3000	2.78	0.8
		300	3000	2.78	0.2
3000	$1\text{Na}^+, 1\text{Cl}^-$	200	3000	2.78	0.8
		300	3000	2.78	0.2

**Table S2: Charge and Lennard-Jones (LJ) parameters** ( $\sigma_{\text{LJ}}$  representing the atomic diameter and  $\epsilon_{\text{LJ}}$ , depth of the potential energy minimum) for the ions used with the TIP4P/2005 water model.

Ion	Charge [ $e$ ]	$\epsilon_{\text{LJ}}$ [kJ/mol]	$\sigma_{\text{LJ}}$ [nm]
$\text{Na}^+$ (Ref. <sup>S6</sup> )	+1	0.0115980	0.333045
$\text{Cl}^-$ (Ref. <sup>S7</sup> )	-1	0.492833	0.441724

final configuration of this simulated annealing run was taken and ions were added randomly in the subsurface, replacing one H<sub>2</sub>O molecule. This system was then equilibrated for 1 microsecond at 200 K.

## S2. A sole NaCl pair in 776H<sub>2</sub>O at various temperatures

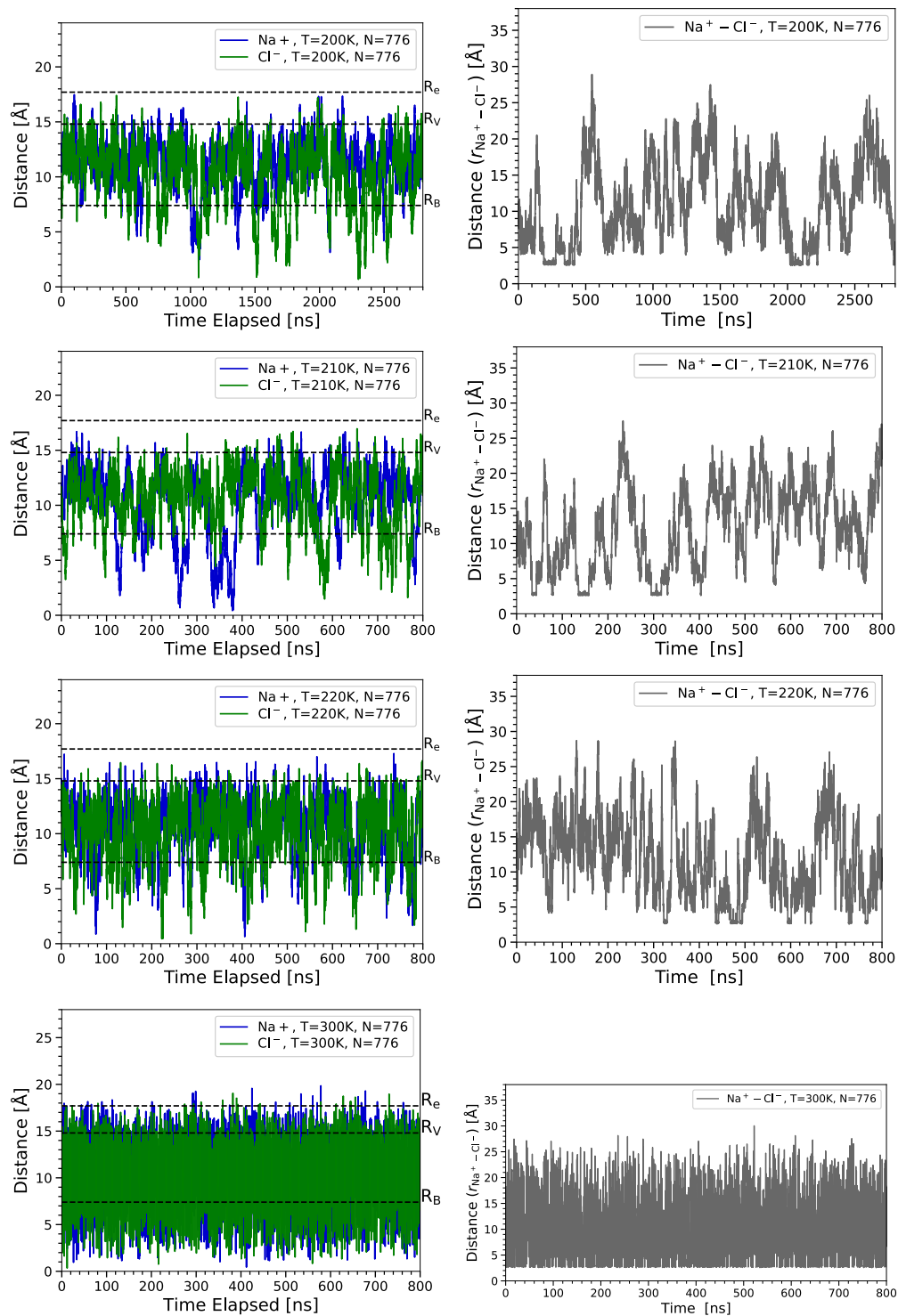
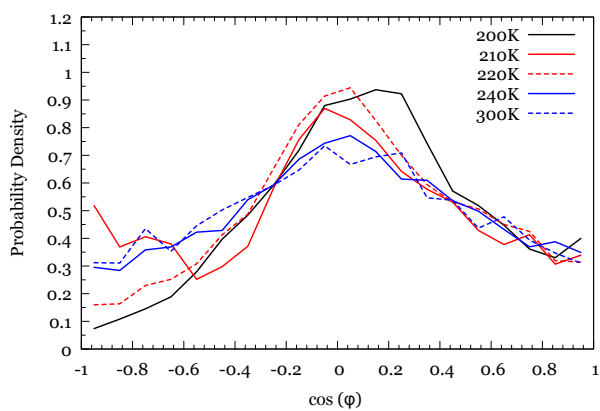
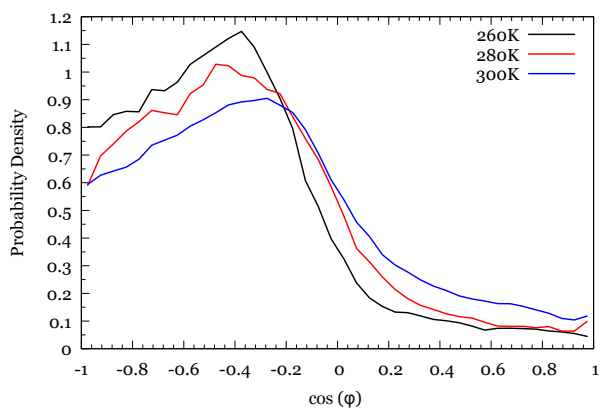


Figure S1: Left column shows the time evolution of the distance of each ion from COM of droplet, and the right column shows the distance between Na<sup>+</sup> and Cl<sup>-</sup>. Simulations are performed with the TIP4P/2005.

### S3. Dipole moment orientation of NaCl



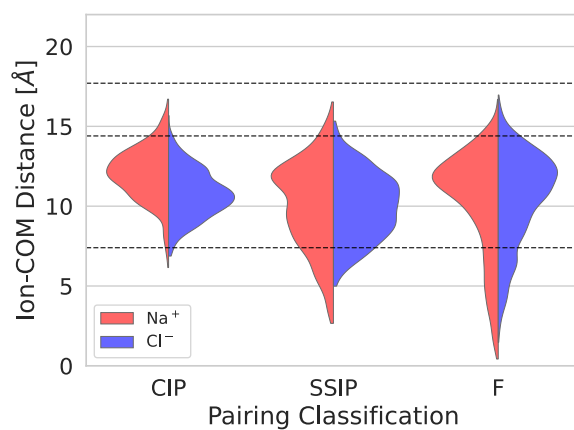
(a)



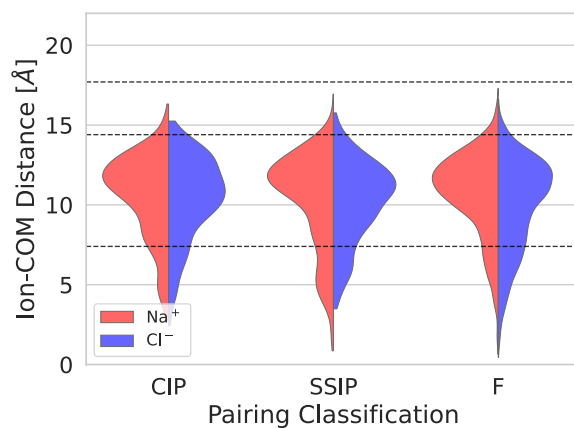
(b)

Figure S2: Dipole moment orientation of NaCl. The dipole moment is defined from the negative site ( $\text{Cl}^-$ ) to the positive site ( $\text{Na}^+$ ). The angle  $\phi$  is defined between the dipole moment and the vector that points from the droplet's COM to the ion-pair COM. (a) TIP4P/2005. (b) SWM4-NDP.

**S4.  $\text{Na}^+$  and  $\text{Cl}^-$  ion-distribution profiles in the CIP, SSIP, and Free Ions forms in a droplet comprising 776 TIP4P/2005  $\text{H}_2\text{O}$  molecules - NaCl at various temperatures**



(a)



(b)

Figure S3: Distribution of  $\text{Na}^+$  (red) and  $\text{Cl}^-$  (blue) sites in the CIP, SSIP and Free ions (F) basins along the distance from the droplet's COM (y-axis) (a) at  $T = 210$  K, (b) at  $T = 220$  K.

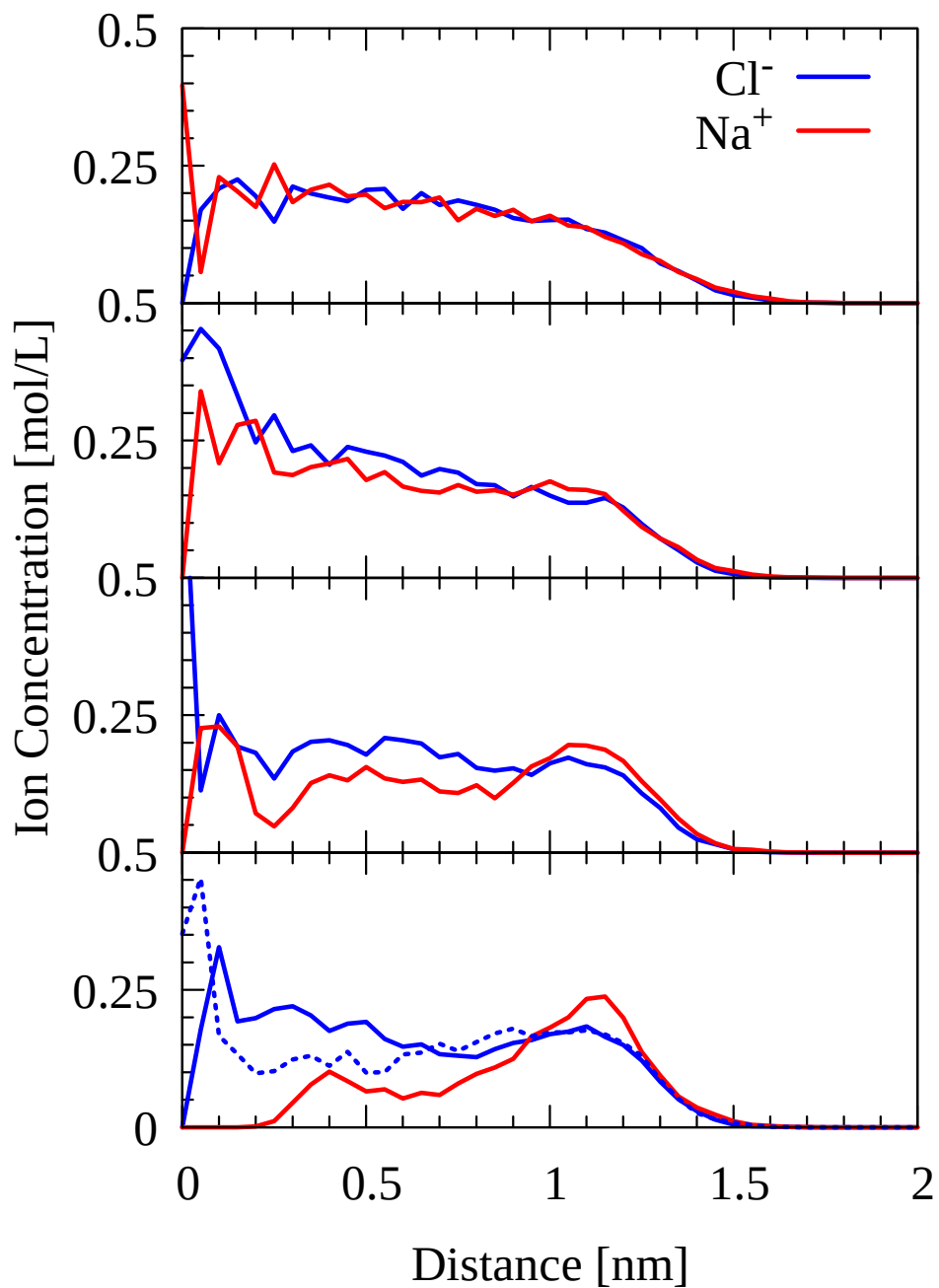
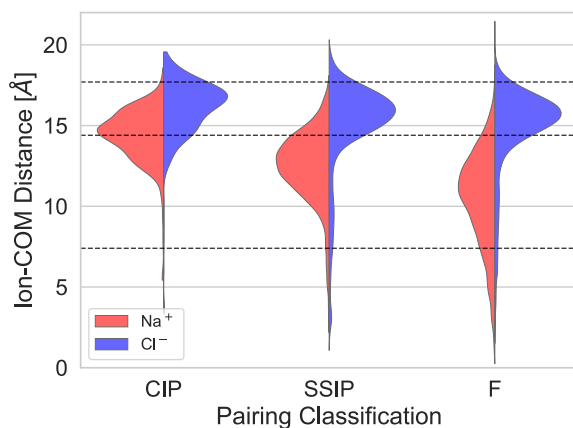
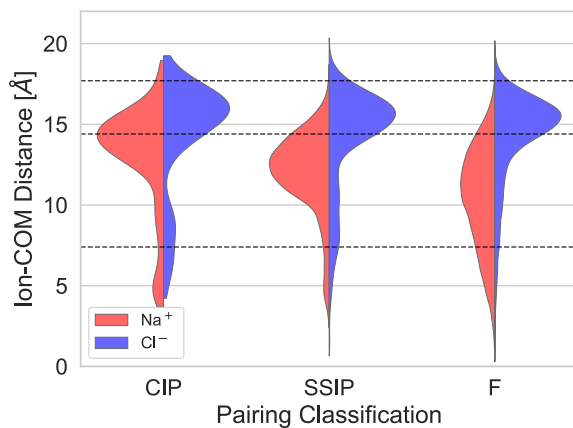


Figure S4: Number density of a Na<sup>+</sup> (red line) and a Cl<sup>-</sup> (blue line) in nanodroplets comprised  $N = 776$  H<sub>2</sub>O molecules and a sole NaCl pair at (a) 300 K; (b) 240 K; (c) 210 K; (d) 200 K. The single Cl<sup>-</sup> (dotted blue) at 200 K is also shown for reference.

**S5.  $\text{Na}^+$  and  $\text{Cl}^-$  ion-distributions in the CIP,SSIP, and (Free Ions) forms in a droplet comprised 776 SWM4-NDP  $\text{H}_2\text{O}$  molecules - NaCl at various temperatures**



(a)



(b)

Figure S5: Distribution of  $\text{Na}^+$  (red) and  $\text{Cl}^-$  (blue) sites in the CIP, SSIP and Free ions (F) basins along the distance from the droplet's COM (y-axis) (a) at  $T = 260$  K, (b) at  $T = 280$  K.

S6.  $\text{Na}^+$  and  $\text{Cl}^-$  location in a 776  $\text{H}_2\text{O}$  at various temperatures using SWM4-NDP

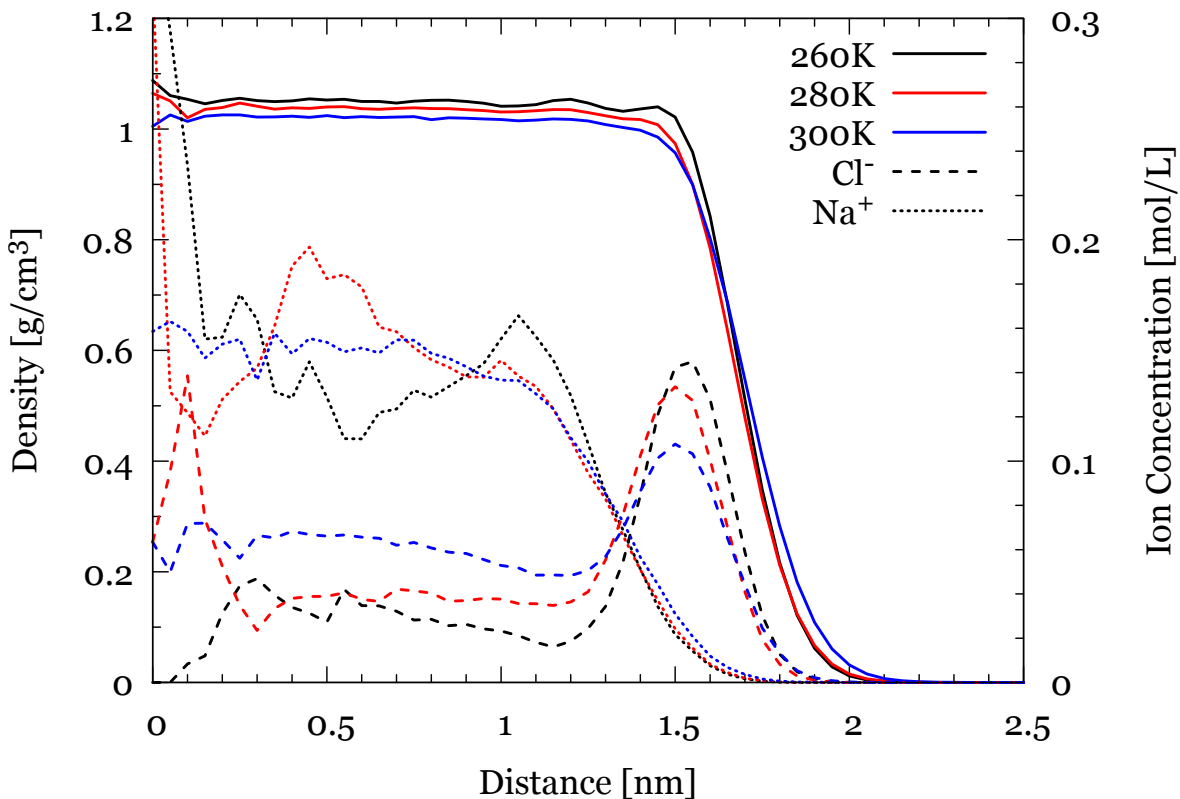


Figure S6: Number density profiles of  $\text{Na}^+$  and  $\text{Cl}^-$  sites (measured in units of concentration in the right y-axis), and  $\text{H}_2\text{O}$  density profiles (measured in units of  $\text{g}/\text{cm}^{-3}$ ) in the left y-axis) at various temperatures in droplets comprising  $N = 776$   $\text{H}_2\text{O}$  molecules and a sole  $\text{NaCl}$  pair. The SWM4-NDP polarizable model is used.

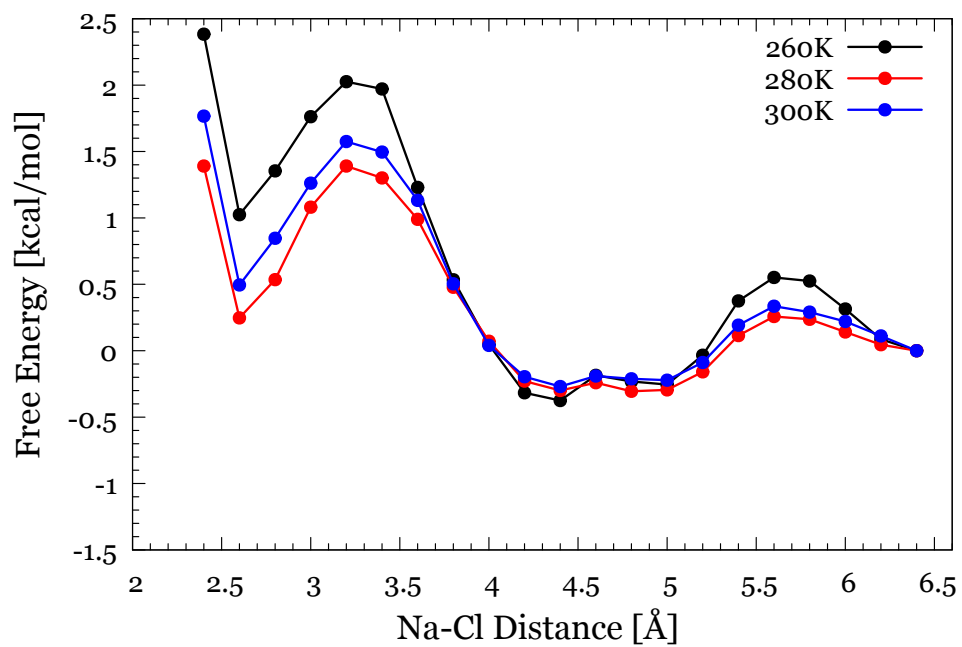


Figure S7: Free energy along the NaCl interionic distance with Langevin damping coefficient 0.01/ps.

# S7. Solvation of $\text{Na}^+$ and $\text{Cl}^-$ in a droplet of 776 SWM4-NDP $\text{H}_2\text{O}$ - $\text{NaCl}$ at 260 K, 280 K, 300 K

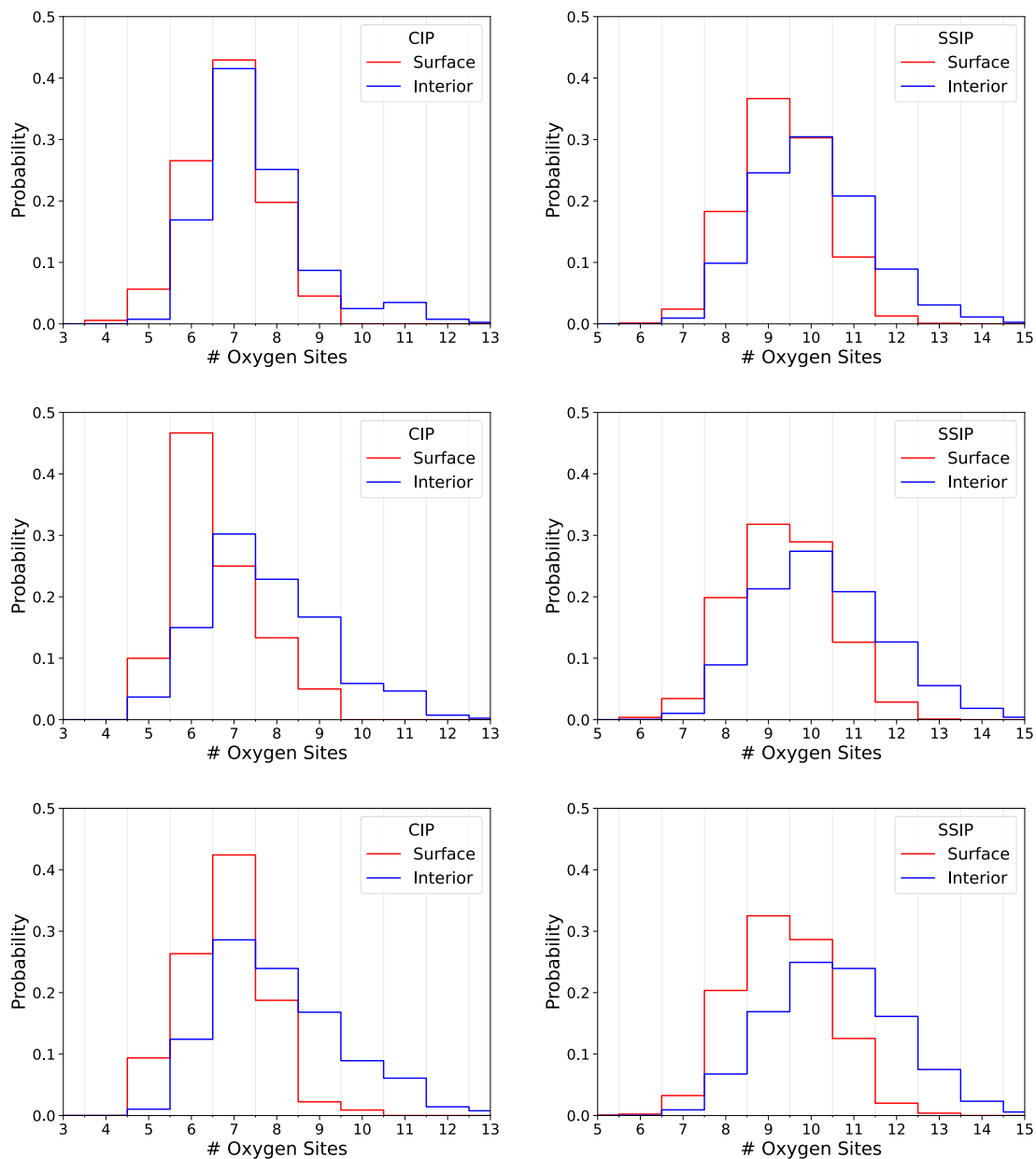


Figure S8: Distribution of the number of oxygen sites in the first solvation shell surrounding the ion pair, modeled by SWM4-NDP. From top to bottom,  $T = 260$  K, 280 K, 300 K. Details are found in the text.

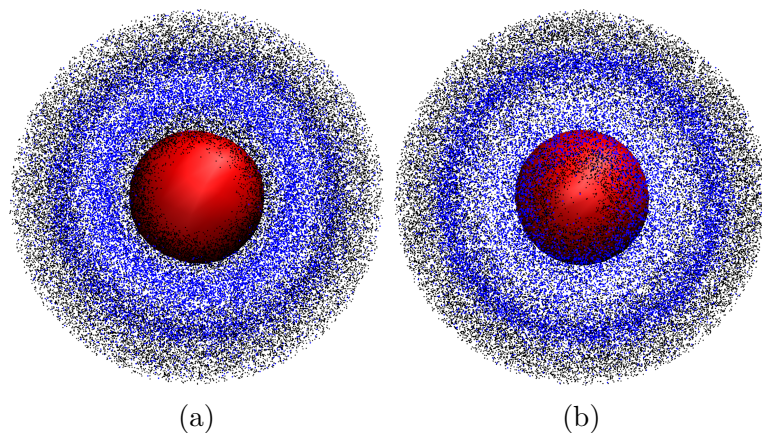


Figure S9: Same as Fig. 4 (a), (c) in the main text but the distribution of the oxygen sites are shown by grey dots and that of the hydrogen sites by blue dots.

S8. 4 NaCl pairs in a droplet of 776 H<sub>2</sub>O molecules modeled by SWM4-NDP

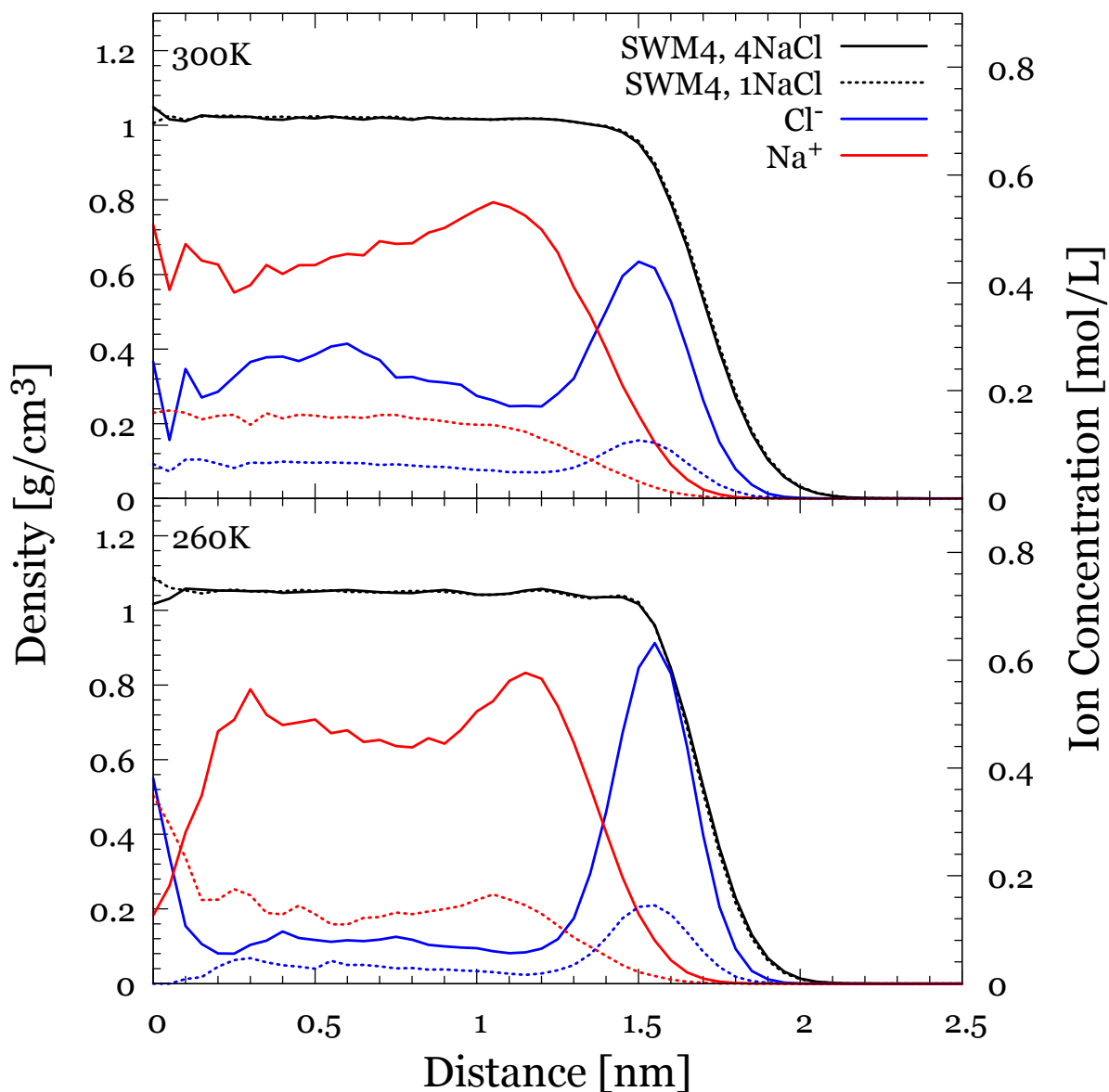


Figure S10: Number density profiles of Na<sup>+</sup> and Cl<sup>-</sup> sites (measured in units of concentration in the right y-axis), and H<sub>2</sub>O density profiles (measured in units of g/cm<sup>-3</sup>) in the left y-axis) at 260 K and 300 K in droplets comprising  $N = 776$  H<sub>2</sub>O molecules and a sole NaCl pair or 4 NaCl pairs. The SWM4-NDP polarizable model is used.

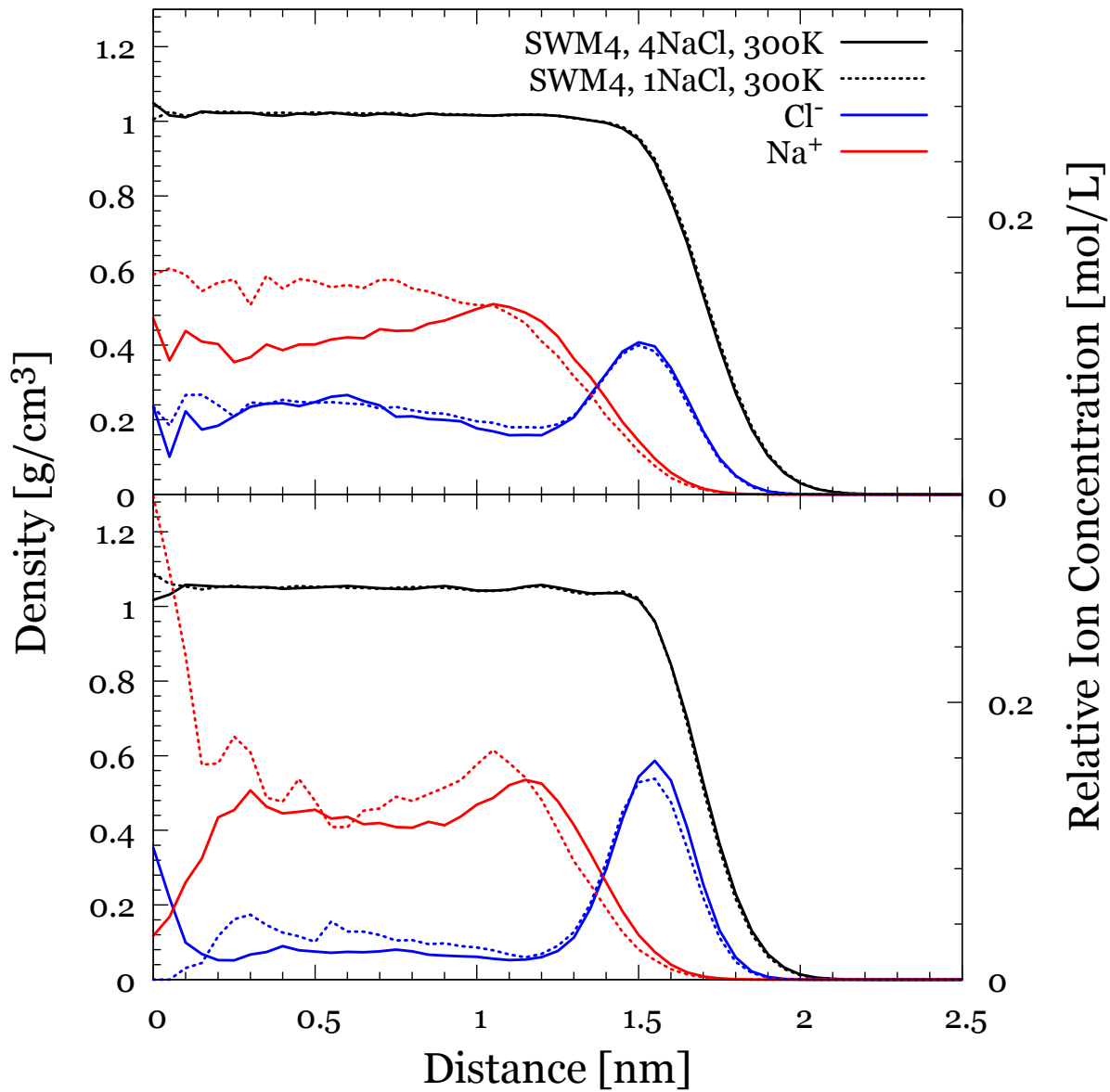


Figure S11: Same as Fig. S10 but the higher salt concentration has been divided by 4.

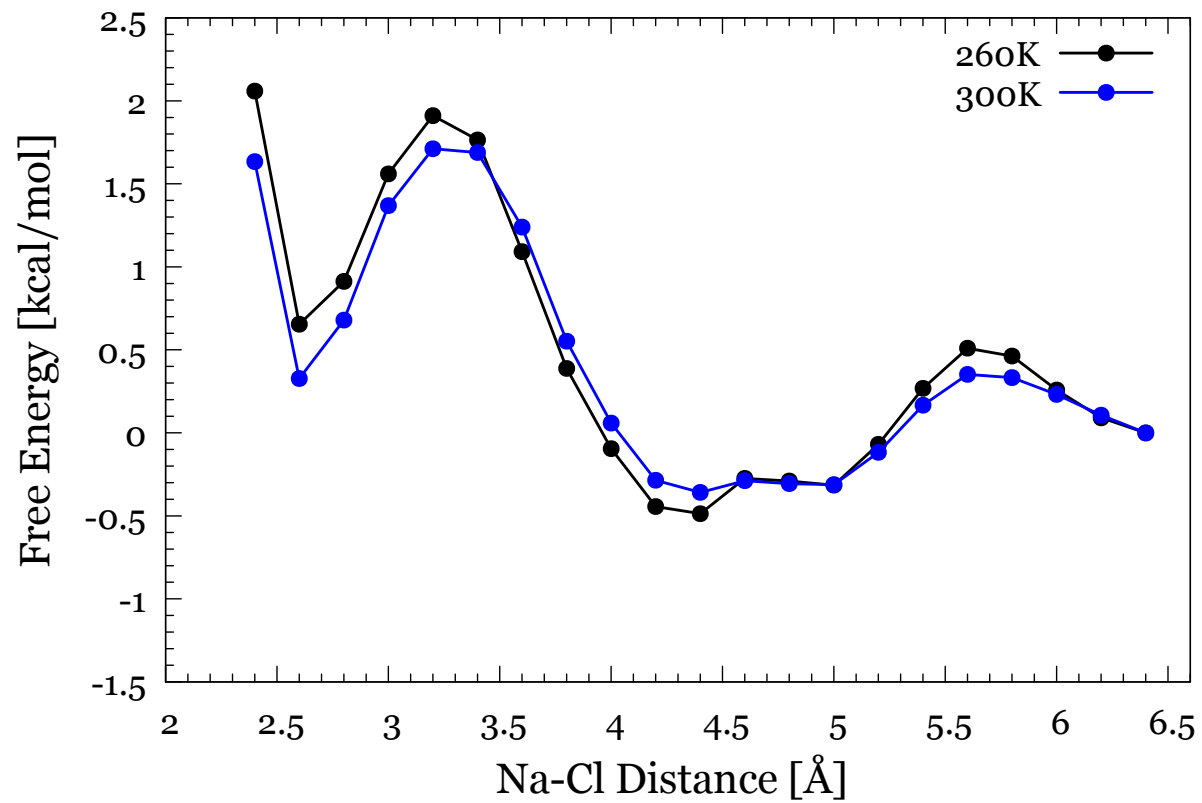


Figure S12: Same as Fig. S10 but the higher salt concentration has been divided by 4.

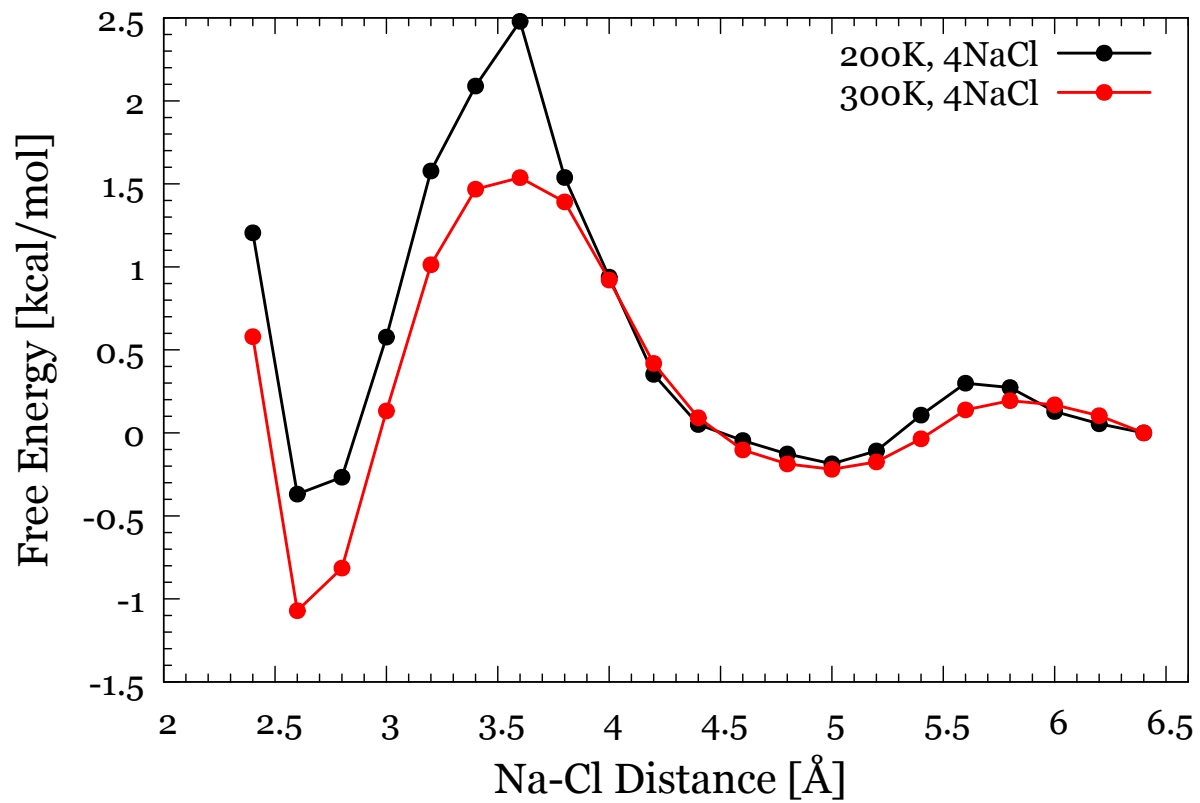


Figure S13: Same as Fig. 2 (a) in the main text but for 4NaCl pairs in  $N = 776$  H<sub>2</sub>O modeled by TIP4P/2005.

## S9. Highly charged droplets with counterions

**Table S3: Integrated number density of the ions in the droplet interior, subsurface and surface in an aqueous droplet with  $N = 3000$   $\text{H}_2\text{O}$  modeled with the TIP4P/2005 set of parameters.**

$T = 240$ K	0 - 18 Å	18Å-27.8Å	27.8Å -
22Na <sup>+</sup>	3.231	18.662	0.107
8Cl <sup>-</sup>	2.591	5.405	0.004
22Cl <sup>-</sup>	3.413	18.541	0.046
8Na <sup>+</sup>	2.621	5.376	0.003
$T = 300$ K	0 - 18 Å	18Å-27.8Å	27.8Å -
22Na <sup>+</sup>	3.632	17.907	0.460
8Cl <sup>-</sup>	2.754	5.233	0.013
22Cl <sup>-</sup>	3.494	17.983	0.249
8Na <sup>+</sup>	2.637	5.243	0.020

Here we extend the studies of the effect of low temperature in the ion location and in their ion-pairing in highly charged supercooled droplets. The study is relevant to native mass spectrometry (MS), where highly charged droplets, generated by spraying, are the intermediate carriers of analytes from the bulk solution to the gaseous state. These droplets disintegrate by solvent evaporation and fission events that release clusters containing solvated ions. The effect of evaporative cooling can be significant in a droplet’s lifetime and as we discuss later, may be exploited to eliminate undesirable salt.

We examine the example of a droplet composed  $3 \times 10^3$   $\text{H}_2\text{O}$  molecules-24 Na<sup>+</sup>-8Cl<sup>-</sup> or 24 Cl<sup>-</sup>-8Na<sup>+</sup>. The systems are modeled by using the TIP4P/2005 set of parameters at 300 K and 240 K. Systems at 200 K were also modelled for over a microsecond time, but no motions of the ions were observed. At  $T = 240$  K the effect of the low temperature was demonstrated and still sampling of the slow dynamics was still feasible. Figure S14 shows the ion distributions at 240 K and 300 K. In droplets greater than a few thousand of  $\text{H}_2\text{O}$  molecules at room or elevated temperature the ions in excess show a maximum near the droplet surface and a slow decay toward the interior. The counterion distribution shows the opposite trend: it is higher in the interior, where the excess ion distribution decays and lower where the excess ion distribution has a maximum. This general trend is expected because

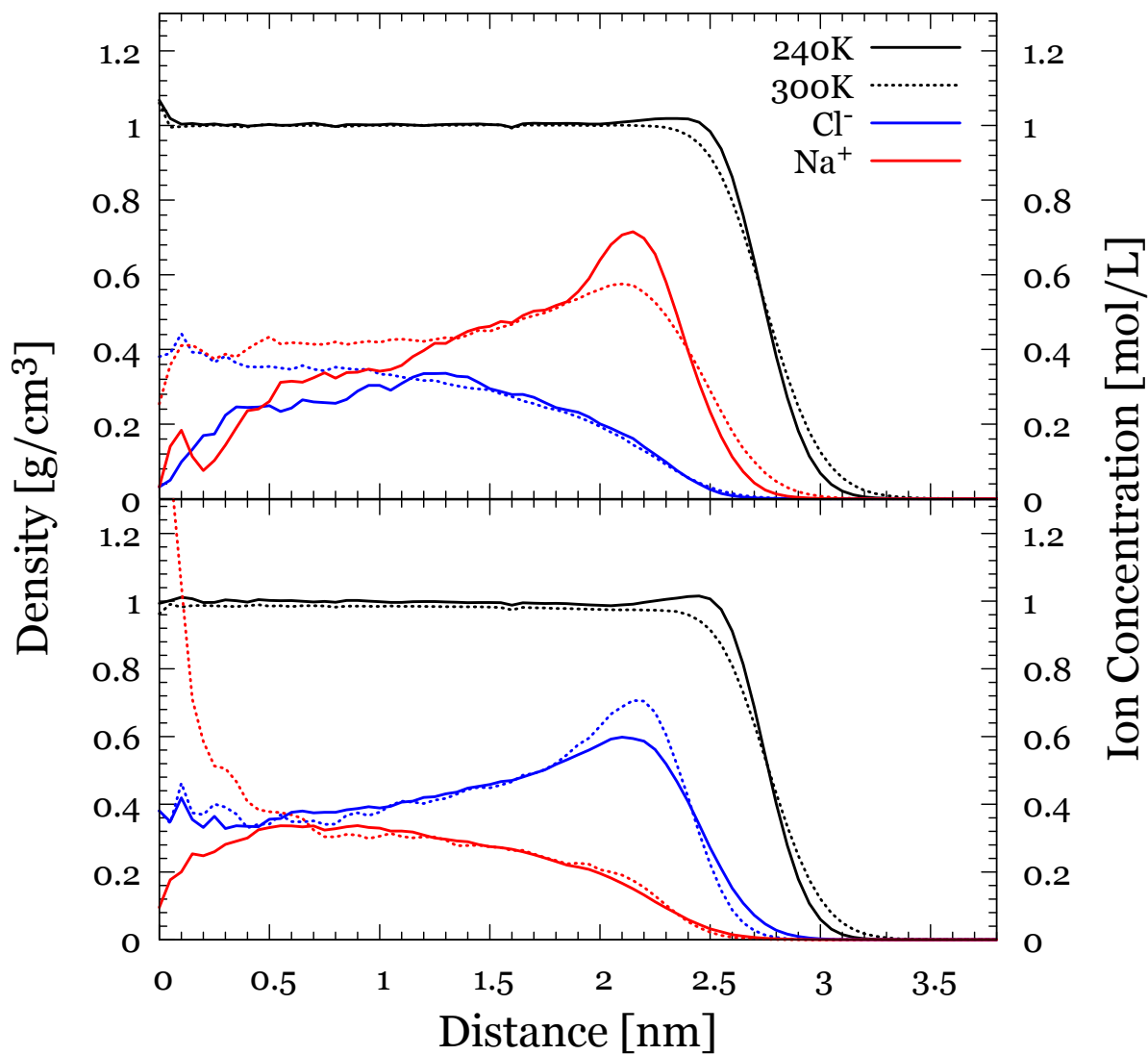


Figure S14: Top: Radial ion density profile for a nanodroplet comprising 3000 H<sub>2</sub>O, 22 Na<sup>+</sup> and 8 Cl<sup>-</sup> (200 ns) bottom: 3000 H<sub>2</sub>O, 8 Na<sup>+</sup> and 22 Cl<sup>-</sup> (200 ns).

the Poisson-Boltzmann equation solved for a sphere where the charge is accumulated on the surface predicts an exponential decay of the ions toward the interior.<sup>S8</sup> In droplets with fewer than 1500 H<sub>2</sub>O molecules the ion-in-excess distribution is almost uniform because (a) the characteristic length of the ion distribution decay is comparable with the droplet radius and (b) the ion distribution is affected by the droplet's large relative shape fluctuations from the spherical shape.<sup>S8</sup>

At 240 K, there is a clear differentiation in the location of the Na<sup>+</sup> and Cl<sup>-</sup> relative to that at 300 K. The majority of the excess ions are accumulated in the subsurface.

We relate our findings in native mass spectrometry processes. In droplet-based ionization methods it is desirable to spray proteins from physiological solution (NaCl or KCl at concentration 150 mM) nevertheless, the formation of adducts of salts with proteins or other macromolecules prevents the use of these conditions. The formation of adducts is avoided by spraying from low ionic strength solutions (40 mM - 70mM), where the ionic strength is provided by ammonium acetate that evaporates by creating volatile molecules NH<sub>3</sub> and CH<sub>3</sub>COOH. Our study suggests that in supercooled droplets the majority of the simple ions may be expelled from the interior to the subsurface. The effect is less pronounced with the TIP4P/2005 model than with the polarizable model. We expect that at lower temperature and with a polarizable model the accumulation of the ions in the surface and subsurface region will be more pronounced. Therefore, by initial cooling a droplet instead of heating, the ions may accumulate near the surface. Possibly, bombardment with other molecules may assist in the detachment of solvated ions or their salt complexes from the surface.

## S10. Dynamics: Diffusion coefficients and representative segments of trajectories

Table S4: Self-diffusion coefficient of H<sub>2</sub>O for TIP4P/2005. See Sec. Dynamics in the main text for details.

Model	$T$ [K]	$D$ [nm <sup>2</sup> /ns]
TIP4P/2005	300	53.1
	260	19.6
	240	10.7
	220	6.01
	210	2.60
	200	0.66

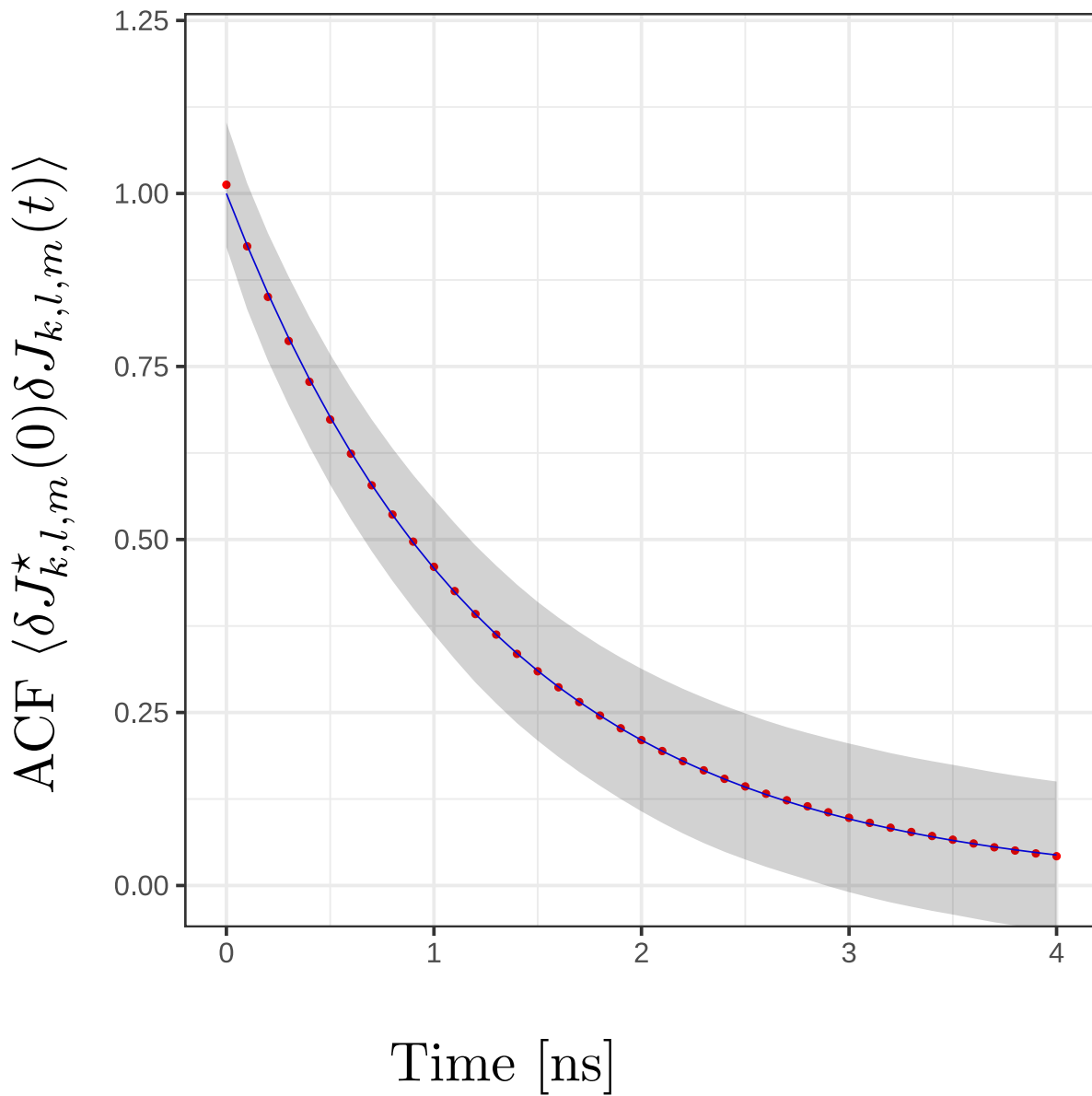
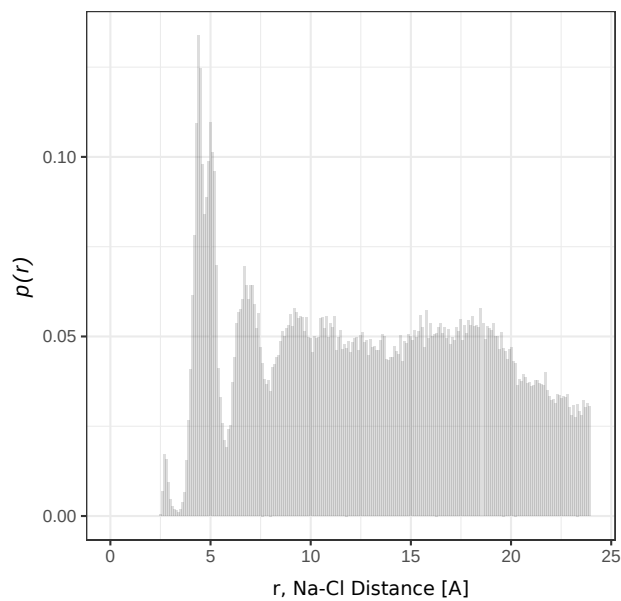
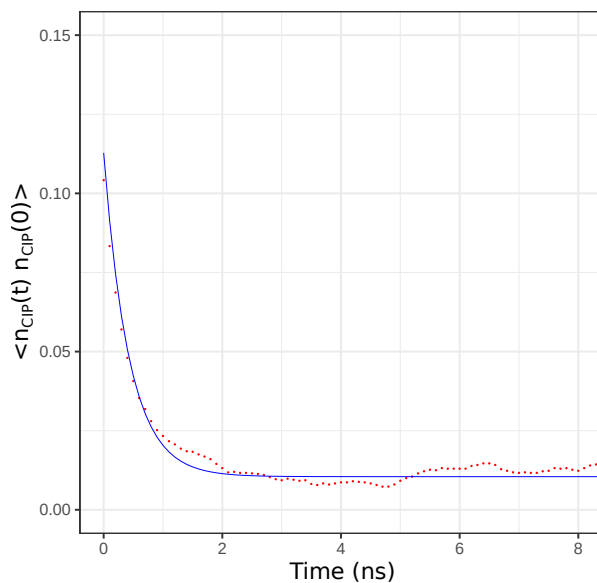


Figure S15: Time correlation function of  $\langle \delta J_{k,l,m}^*(0) \delta J_{k,l,m}(t) \rangle$  in a droplet with  $N = 776$  at  $T = 260$  K modeled by TIP4P/2005. The blue line is the fitting to the simulation data, shown by red points.



(a)



(b)

Figure S16: (a) Histogram of the probability density of the Na-Cl interionic distance in a droplet with  $N = 776$  at  $T = 260$  K modeled by TIP4P/2005. (b) Autocorrelation function of the state variable  $n_{\text{CIP}}(t)$  for the same system. The blue line is the fitting to the simulation data shown by red points.



## References

- (S1) Phillips, J. C.; Braun, R.; Wang, W.; Gumbart, J.; Tajkhorshid, E.; Villa, E.; Chipot, C.; Skeel, R. D.; Kalé, L.; Schulten, K. Scalable molecular dynamics with NAMD. *J. Comput. Chem.* **2005**, *26*, 1781–1802.
- (S2) Malek, S. M. A.; Kwan, V.; Saika-Voivod, I.; Consta, S. Low density interior in supercooled aqueous nanodroplets expels ions to the subsurface. *J. Am. Chem. Soc.* **2021**, *143*, 13113–13123.
- (S3) Lamoureux, G.; Harder, E.; Vorobyov, I. V.; Roux, B.; MacKerell, A. D. A polarizable model of water for molecular dynamics simulations of biomolecules. *Chem. Phys. Lett.* **2006**, *418*, 245–249.
- (S4) Yu, H.; Whitfield, T. W.; Harder, E.; Lamoureux, G.; Vorobyov, I.; Anisimov, V. M.; MacKerell, A. D.; Roux, B. Simulating Monovalent and Divalent Ions in Aqueous Solution Using a Drude Polarizable Force Field. *J. Chem. Theory Comput.* **2010**, *6*, 774–786, PMID: 20300554.
- (S5) Luo, Y.; Jiang, W.; Yu, H.; MacKerell, A. D.; Roux, B. Simulation study of ion pairing in concentrated aqueous salt solutions with a polarizable force field. *Faraday Discuss.* **2013**, *160*, 135–149.
- (S6) Aqvist, J. Ion-water interaction potentials derived from free energy perturbation simulations. *J. Phys. Chem.* **1990**, *94*, 8021–8024.
- (S7) Chandrasekhar, J.; Spellmeyer, D. C.; Jorgensen, W. L. Energy component analysis for dilute aqueous solutions of lithium(1+), sodium(1+), fluoride(1-), and chloride(1-) ions. *J. Am. Chem. Soc.* **1984**, *106*, 903–910.
- (S8) Kwan, V.; Consta, S. Bridging electrostatic properties between nanoscopic and microscopic highly charged droplets. *Chem. Phys. Lett.* **2020**, 137238.